Hydrogen Production From Biomass Derived Compounds

Dube Tapiwanashe

Thesis for MSc Petroleum And Mining Engineering

Supervisors:

Prof De Chen (NTNU)
Prof Raffaele Pirone (Polito)
Prof Edd Blekkan (NTNU)
Dr Ainara Moral Larrasoana (NTNU)

July 4, 2023

Abstract

This thesis presents a study on the production of hydrogen through ethanol steam reforming. The objective of this study was to investigate the kinetics of the ethanol steam reforming reaction. The primary focus was to identify the most suitable catalyst for this reaction based on its kinetic properties.

Two different catalyst compositions, namely a cobalt-nickel alloy with a ratio of 35% cobalt and 5% nickel (referred to as 35Co05Ni catalyst) and a cobalt-nickel alloy with equal proportions of 20% cobalt and 20% nickel (referred to as 20Co20Ni catalyst), were employed for the experiments.

The obtained results indicated that the utilization of the 20Co20Ni catalyst resulted in a determined reaction order of 0.92 for ethanol, while the 35Co05Ni catalyst exhibited a reaction order of 1.06. The reaction order signifies the relationship between the concentration of the reactants and the rate of the reaction. A reaction order close to 1 suggests a linear relationship, wherein a doubling of the reactant concentration leads to approximately a doubling of the reaction rate.

Additionally, the activation energy values were determined to be 85.9 kJ/mol for 20Co20Ni catalyst and 135.9 kJ/mol for 35Co05Ni catalyst. Activation energy is a measure of the energy barrier that must be overcome for a chemical reaction to occur. A lower activation energy indicates that the reaction can proceed at a faster rate, as less energy is required for the reactant molecules to reach the necessary threshold.

Based on these findings, it is recommended to employ the 20Co20Ni catalyst for the production of hydrogen through ethanol steam reforming. The 20Co20Ni catalyst demonstrated a lower activation energy in comparison to the 35Co05Ni catalyst. This indicates that the 20Co20Ni catalyst enables a more efficient conversion of ethanol to hydrogen, resulting in a higher reaction rate and reduced energy demand. Consequently, the use of the 20Co20Ni catalyst is expected to optimize the efficiency of the ethanol steam reforming process.

Preface

This master thesis was performed at the Norwegian University of Science and Technology (NTNU). It has been done at the Department of Chemical Engineering and Catalysis Group from July to December of 2022.

I would like to express my heartfelt gratitude to Dr. Ainara Moral Larrasoana for her invaluable guidance, support, and constant presence throughout my research journey. Her tireless efforts, day and night, including weekends, were instrumental in bringing this project to fruition. Without her, I would not have been able to complete my master's thesis, and for that, I am deeply grateful.

I am also grateful to the engineers who provided me with their technical expertise and unwavering support during the course of my research. Their dedication had played a significant role in overcoming the numerous obstacles that I had faced. A special shout-out goes to Estelle, whose warm welcome and kind-heartedness made me feel at home when I arrived at NTNU. Her support and encouragement gave me the confidence to proceed with my research, for which I am truly thankful.

In addition to that, I am indebted to the services of countless Ph.D. students who were always there to provide me with prompt assistance whenever needed. Among them, I would like to give a special mention to Oscar, whose exceptional support and guidance during my research have been critical in shaping my academic career. The dedication, technical expertise, and valuable inputs that I received from the Ph.D. students were incredibly priceless, for which I feel obliged to extend my heartfelt appreciation.

I hereby declare that this is an independent work according to the exam regulations of the Norwegian University of Science and Technology and Polytechnic University of Turin.

Turin, 24 April 2023

Dube Tapiwanashe

Contents

1 Summary **1**

2 Introduction **2**

3 Objective **3**

4 Catalytic Study **4**
4.1 Reaction Mechanism 4
4.2 Types of catalysts 7
4.2.1 Noble metal catalysts 7
4.2.2 Non-noble metal catalysts 10
4.3 Catalyst Preparation 13
4.4 Catalyst Characterization 14
4.5 Thermal Analysis 18
4.6 Physical–Chemical Properties 20
4.7 Temperature Programmed Reduction 21
4.8 STEM and EDS Mapping 23
4.9 Catalyst Testing 24
4.10 Sintering 27
4.11 Promoter effect on Ni-Co bimetallic catalysts 28

5 Description of the installation **30**

6 Kinetic Theory **32**
6.1 Conversion 32
6.2 Reaction Rate 33
6.3 Power Rate Law 34
6.4 Turnover frequency (TOF) 35
6.5 Arrhenius Equation 35

7 Results and Discussion **37**
7.1 Transport limitations 37
7.1.1 Internal Transport Limitation 37
7.1.2 External Transport Limitation 38
7.2 Ethanol Reaction Order 39
7.2.1 Results for 20Co20Ni/HT catalyst 40
7.2.2 Results for 35Co05Ni/HT catalyst 44
7.2.3 Conclusion 47
7.3 Hydrogen Reaction Order 49
7.3.1 Results for 20Co20Ni/HT catalyst 50
7.3.2 Results for 35Co05Ni/HT catalyst 52
7.3.3 Conclusion 55
7.4 Activation Energy 56
7.4.1 Conclusion 60

8 Results Confirmation **61**

9 Deactivation of Nickel-based catalyst **62**

10 Conclusion **65**

1 Summary

Hydrogen is considered a key player in the fight against climate change as it is a clean fuel that produces no harmful emissions when used in fuel cells or combustion engines. Ethanol steam reforming is a promising method for the production of hydrogen, as it allows the use of renewable ethanol as a feedstock and generates high-purity hydrogen with a high energy density.

Catalysts play a critical role in the efficiency and selectivity of ethanol steam reforming, as they facilitate the chemical reactions involved and control the formation of byproducts. This thesis aims to study the kinetics of 35Co05Ni and 20Co20Ni catalysts for ethanol steam reforming to produce hydrogen and determine which one is more suitable for this process.

The experiments were designed to determine the reaction order of hydrogen and ethanol, as well as the activation energy of the 35Co05Ni and 20Co20Ni catalysts. These parameters were used to compare the performance of the two catalysts and identify the best performer for ethanol steam reforming.

Catalyst deactivation due to carbon deposition is a major challenge in this process. To address this challenge we studied the effect of hydrotalcite (HT)-like material support on Ni-Co bimetallic catalysts for ethanol steam reforming to produce hydrogen. The data indicated that the use of HT-like material support was successful in neutralizing the acidity of the support material and reducing coking in ethanol steam reforming.

Further analysis of the data indicated that 20Co20Ni catalyst had a lower activation energy compared to 35Co05Ni catalyst. This means that 20Co20Ni catalyst is more favorable for ethanol steam reforming, as it requires less energy to initiate the reaction.

The findings of this thesis highlight the importance of catalyst selection and optimization for the efficient and sustainable production of hydrogen from ethanol steam reforming. The results demonstrate that 20Co20Ni catalyst is the better performer between the two due to its lower activation energy. This information can guide the development of improved catalysts for this process and promote the use of renewable feedstocks for hydrogen production.

2 Introduction

The world faces a major challenge in finding alternative sources of energy that do not contribute to climate change. Currently, the majority of the world's energy supply is derived from fossil fuels such as coal, which is a significant source of greenhouse gases. This underscores the need to transition towards cleaner sources of energy [1]. Furthermore, energy consumption is expected to increase in the near future due to population growth, an increase in living standards, and industrialization [2]. Consequently, it is essential to urgently shift towards renewable energy sources to mitigate global warming.

Sustainable hydrogen has been proposed as the key element in achieving a decarbonized society, and a rapid transition towards a hydrogen-based ecosystem is consistent with the goal of attaining Carbon Neutrality by 2050 and the Agenda 2030 for sustainable development [3]. Hydrogen applications offer solutions to problems associated with carbon dioxide emissions into the atmosphere, including global warming. It can be utilized for transportation, power generation, oil refineries, petrochemicals, ammonia production, methanol production, steel industry, and heating buildings [4].

Currently, natural gas constitutes approximately 75 percent of the total hydrogen production worldwide [5]. However, technologies such as steam methane reforming, partial oxidation, and methane pyrolysis are not sustainable or carbon-neutral methods of production. The environmental impact of producing and transporting natural gas to conversional facilities needs to be considered due to their contribution to global warming.

At present, one of the primary areas of research in sustainable energy is the development of efficient, sustainable, and environmentally-friendly methods for producing hydrogen from biomass-derived compounds. Various methods are currently being investigated, such as gasification, pyrolysis, aqueous phase reforming, biological water gas shift, dark fermentation, photo-fermentation, and electrochemical processes.

3 Objective

The Catalysis Group (KinCat) at the Norwegian University of Science and Technology (NTNU) has conducted an investigation on a series of Co-Ni catalysts for hydrogen production through ethanol steam reforming.

At NTNU, my research involves planning and conducting experiments on steam reforming to produce hydrogen from ethanol using Co-Ni catalysts prepared through co-precipitation techniques and derived from hydrotalcite (HT)-like materials.

The aim of my research is to conduct a kinetic study comparing the performance of two catalysts, namely 35Co05Ni/HT and 20Co20Ni/HT, for hydrogen production through the catalytic steam reforming of ethanol. The study aims to determine which catalyst exhibits superior performance in terms of key metrics such as conversion efficiency, hydrogen yield, and stability under reaction conditions. By assessing these factors, we seek to identify the catalyst that achieves the highest overall effectiveness for hydrogen production in this specific reaction system.

4 Catalytic Study

4.1 Reaction Mechanism

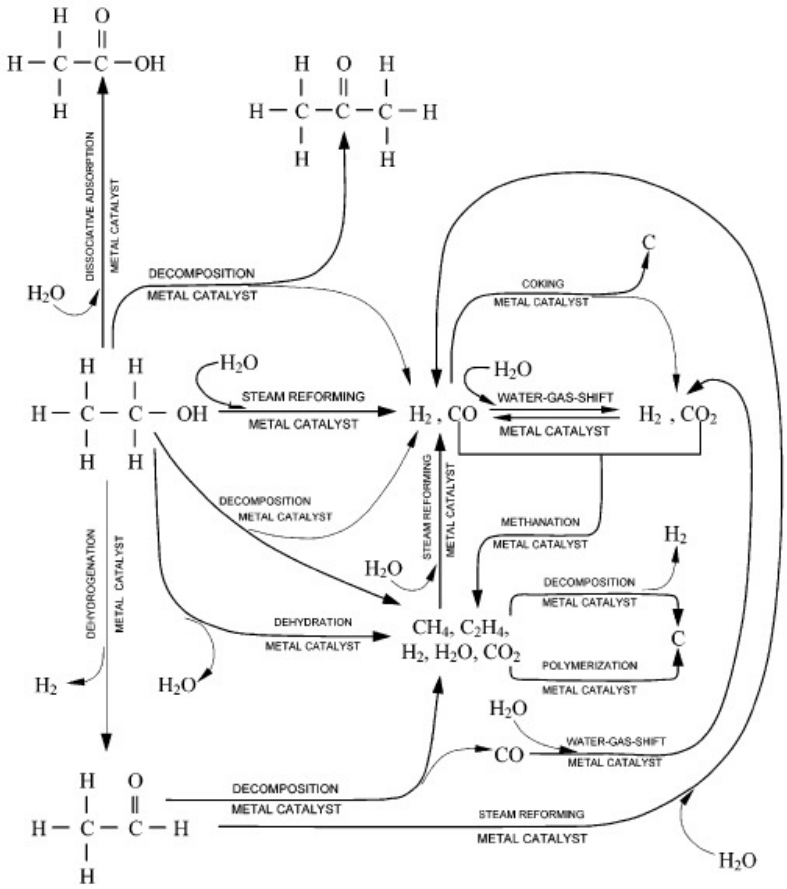

Figure 1: Reaction pathways that can occur during ethanol steam reforming over metallic catalysts [6].

The direction of ethanol steam reforming is known to depend on the type of catalyst employed. Figure 1, adapted from the literature, provides an illustration of the various reactions involved in this process, serving as a foundational reference for our study.

Reactions are as follows:

1. Ethanol dehydration to ethylene and water followed by polymerization of ethylene to form coke.

dehydration:

$$C_2H_5OH \longrightarrow C_2H_4 + H_2O \qquad (1)$$

polymerization:

$$C_2H_4 \longrightarrow \text{coke} \qquad (2)$$

2. Ethanol decomposition or cracking to ethane, followed by steam reforming.
decomposition:

$$C_2H_5OH \longrightarrow CH_4 + CO + H_2 \qquad (3)$$

steam reforming:

$$CH_4 + 2\,H_2O \longrightarrow 4\,H_2 + CO_2 \qquad (4)$$

3. Ethanol dehydrogenation to acetaldehyde, followed by decarbonylation or steam reforming to acetaldehyde.
dehydrogenation:

$$C_2H_5OH \longrightarrow C_2H_4O + H_2 \qquad (5)$$

decarbonylation:

$$C_2H_4O \longrightarrow CH_4 + CO \qquad (6)$$

steam reforming:

$$C_2H_4O + H_2O \longrightarrow 3\,H_2 + 2\,CO \qquad (7)$$

4. Ethanol decomposition into acetone, followed by steam reforming.
decomposition:

$$2\,C_2H_5OH \longrightarrow CH_3COCH_3 + CO + 3\,H_2 \qquad (8)$$

steam reforming :

$$CH_3COCH_3 + 2\,H_2O \longrightarrow 5\,H_2 + 3\,CO \qquad (9)$$

5. Steam reforming of ethanol to syngas.
steam reforming:

$$C_2H_5OH + H_2O \longrightarrow 2\,CO + 4\,H_2 \qquad (10)$$

6. Water gas shift:

$$CO + H_2O \longrightarrow CO_2 + H_2 \qquad (11)$$

7. Methanation:

$$CO + 3\,H_2 \longrightarrow CH_4 + H_2O \qquad (12)$$

$$CO_2 + 4\,H_2 \longrightarrow CH_4 + 2\,H_2O \qquad (13)$$

8. Coking from decomposition of methane:

$$CH_4 \longrightarrow 2\,H_2 + C \qquad (14)$$

9. Coking from the Boudouard reaction:

$$CO_2 \longrightarrow O_2 + C \qquad (15)$$

10. Dissociative adsorption of water to form acetic acid:
water adsorption:

$$C_2H_5OH + H_2O \longrightarrow CH_3COOH + 2\,H_2 \qquad (16)$$

Stoichiometrically, the overall equation for ethanol steam reforming is as follows:

$$C_2H_5OH + 3\,H_2O \longrightarrow 2\,CO_2 + 6\,H_2 \qquad (17) \quad \Delta H_{298^\ominus} = 174 \text{ KJ mol}^{-1}$$

Table 1
Ethanol steam reforming reaction pathways [7].

Reaction	Equation	Remarks
Sufficient steam supply	(17)	Ideal pathway, highest hydrogen production
Insufficient steam supply	(10)	Undesirable products,lower hydrogen production
Dehydration	(1)	Undesired pathway, main source of coke formation
Polymerization	(2)	
Decomposition	(8)	Coke formation, low hydrogen production
	(3)	
Reaction of decomposition products		
Methanation	(12)	
	(13)	
Decomposition of Methane	(14)	
Boudouard reaction	(15)	
Water gas shift reaction	(11)	Reduce coke formation, increases hydrogen production

4.2 Types of catalysts

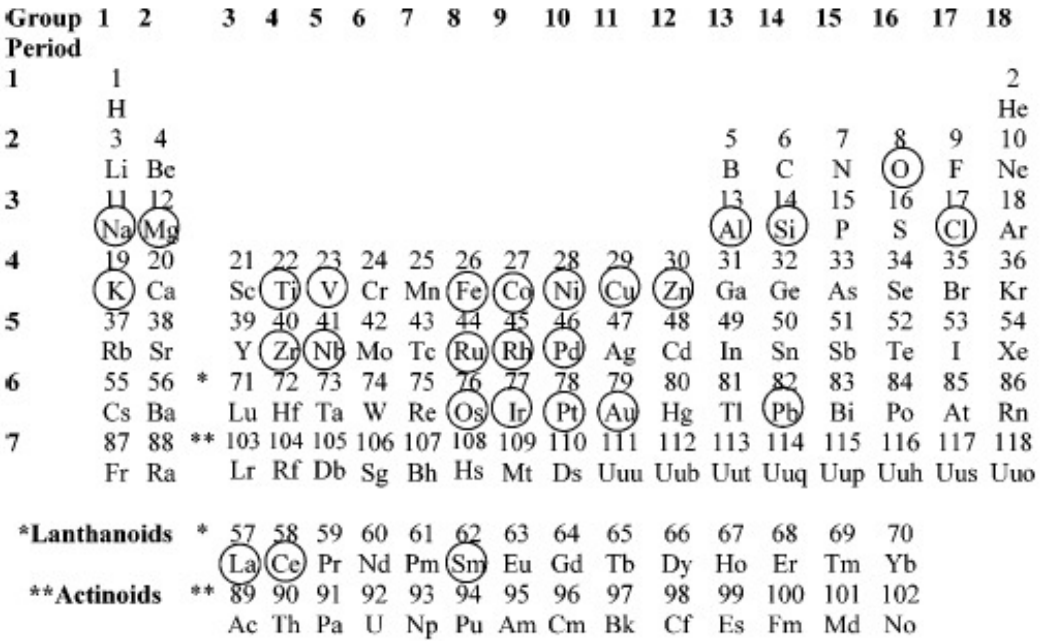

Figure 2: Examples of compounds that were investigated as catalysts in ethanol reforming (shown in circles) [6].

4.2.1 Noble metal catalysts

Previous studies have investigated Rh, Ru, Pd, and Pt as catalysts for ethanol steam reforming and found them to be highly active. Liguras et al [8] conducted a comparison of the catalytic performance of these catalysts at temperatures ranging from 873 to 1123 K, revealing that Rh exhibited the best catalytic performance in terms of ethanol conversion and hydrogen production. Although Ru was inactive at low loading, it showed comparable catalytic activity to Rh at high loading. The use of a 5 wt percent Ru/Al2O3 catalyst resulted in complete conversion of ethanol to syngas with a hydrogen selectivity of over 95 percent. Catalyst atom dispersion at the support surface was found to be crucial in enhancing catalyst activity. The selection of a suitable support material also played a critical role in ensuring long-term catalyst stability. Ethanol dehydration induced by acidic supports led to the production of ethylene, which was a significant source of coke formation (as indicated in Table 1).

In previous studies, researchers such as Frusteri et al. [9] investigated the effectiveness of various catalysts, including Pd, Rh, Ni, and Co, supported on MgO, for hydrogen production via ethanol steam reforming. Among these, Rh/MgO demonstrated the highest catalytic activity and stability in terms of ethanol conversion, while Ni/MgO exhibited hydrogen selectivity of over 95 percent. The low coke formation rate on Rh/MgO can be attributed to the basic nature of MgO. However, it was observed that the deactivation of the catalyst was primarily due to metal sintering.

Erdohelyi et al. [10] carried out a study comparing the effects of ethanol steam reforming on noble metal catalysts supported by Al2O3 and CeO2, namely Pt, Ir, Pd, Rh, and Ru. The researchers analyzed the surface species formed during ethanol adsorption on the supported catalysts and found that water had a stabilizing effect on the ethoxide surface species formed during the ethanol dissociation process. Ethylene, resulting from the dehydration of ethanol, was detected on Al2O3-supported noble metal catalysts, while CeO2-supported catalysts produced acetaldehyde via ethanol dehydrogenation. Furthermore, the study showed that hydrogen production decreased over time on CeO2-supported noble metal catalysts due to the inhibitory effect of surface acetate species formed on the support. This investigation provided valuable insights into the reaction mechanisms involved in ethanol steam reforming and enhanced our understanding of the chemical processes taking place on the catalyst surfaces.

Rhodium deposition on MgAl-based spinel oxide supports resulted in higher basicity compared to Rh deposition on alumina supports, leading to improved stability due to reduced surface acidity [11]. The addition of Ni to Rh supported on CeO2 in a bimetallic catalyst was found to enhance the dispersion of Rh particles, resulting in higher catalytic activity. Additionally, the use of smaller crystals of CeO2 support improved the interaction between Rh and CeO2 [12]. Unlike Rh, the co-deposition of Pd and Zn on a ZnO support resulted in the formation of a PdZn alloy that favored dehydrogenation and hydrogen production [13].

Figure 3 demonstrates that, in general, Rh is a more effective catalyst for hydrogen production through ethanol steam reforming compared to other noble metals such as Pt, Pd, and Au. At high temperatures and catalyst loadings, Ru displays similar performance to Rh. Among the suitable supports for efficient ethanol reforming on Rh, CeO2, MgO, and La2O3 are highlighted. However, the use of Al2O3 as a support leads to significant catalyst deactivation during long-term

operation. In terms of long-term stability, MgO is found to exhibit the best performance. The findings suggest that La2O3 may also be a promising support for Rh in achieving stable ethanol steam reforming.

Table 2
List of ethanol steam reforming using noble metal catalyst

Catalyst	Support	Temperature (K)	Steam/Ethanol molar ratio	Ethanol conversion (%)
Rh (1 wt%)	γ-Al_2O_3	1073	3:1	100
(2 wt%)				100
Ru (1 wt%)				42
(5 wt%)				100
Pt (1 wt%)				60
Pd (1 wt%)				55
Rh (5 wt%)	γ-Al_2O_3		8.4:1	100% at the beginning 43% 100 h after operation
Rh (3 wt%)	MgO	923	8.5:1	99 (10 h)
Pd (3 wt%)				10 (10 h)
Ni (21 wt%)				42 (10 h)
Co (21 wt%)				55 (10 h)
Ru (1 wt%)	CeO_2	723	Not known	Above 90%
Rh (1 wt%)				
Rh (2 wt%)	CeO_2	573	8:1	58.5
		673		100
		723		100
	ZrO_2	573		100
		723		100

Figure 3: List of ethanol steam reforming using noble metal catalyst [7].

4.2.2 Non-noble metal catalysts

Sun et al. [14] conducted a comparative study on the catalytic activity of Ni/Y2O3, Ni/La2O3, and Ni/Al2O3 for hydrogen production via ethanol steam reforming. The catalysts were prepared using nickel oxalate as a precursor and impregnation-decomposition-reduction method. Operating at ambient pressure and at 593 K, Ni/Y2O3 and Ni/La2O3 exhibited ethanol conversion of 93.1 percent and 99.5 percent, respectively, while the selectivity of hydrogen was 53.2 percent and 48.5 percent, respectively. The high activity and stability of Ni/La2O3 were attributed to the formation of a lanthanum oxycarbonate species (La2O2CO3), which could react with surface carbon deposited during the reaction to prevent catalyst deactivation. In contrast, the selectivity of hydrogen for Ni/Al2O3 catalyst reached a maximum of 47.7 percent at 573 K, which was relatively low, probably due to the low water/ethanol molar ratio used (3:1). It was demonstrated that increasing the water/ethanol molar ratio could significantly increase the selectivity of hydrogen [15].

Aside from La2O3 and Al2O3, other oxides have been explored as alternative supports for Ni catalysts. Yang et al. [16] investigated the effect of support on ethanol steam reforming using Ni-based catalysts. At a Ni loading of 10 wt percent, all catalysts achieved almost

100 percent conversion of ethanol at 923K. Frusteri et al. [17] examined the impact of alkali addition (Li, Na, and K) on the catalytic performance of Ni/MgO. The addition of Li and K improved catalyst stability by inhibiting Ni sintering. Coke formation was found to be faster on Ni/CeO2 than on Ni/MgO [18]. This observation was attributed to the strong interaction of CeO2 support with the adsorbed reaction intermediate species. Moreover, their tests revealed that the basic nature of MgO favored ethanol reforming and reduced coke formation.

In a study by Akande et al. [19], the catalytic activity of Ni/Al2O3 catalysts for ethanol reforming was investigated with respect to the synthesis method, Ni loading, and temperature. The study used a water/ethanol molar ratio of 13:1, which represents the actual composition of bio-ethanol produced from biomass fermentation. Three preparation methods were evaluated: co-precipitation, precipitation, and impregnation. The optimal Ni loading of 15 percent was found for maximum ethanol conversion using Ni/Al2O3 catalysts prepared by co-precipitation and precipitation methods. However, the Ni loading did not significantly affect the Ni/Al2O3 activity when the impregnation method was used. The catalyst prepared by co-precipitation with a Ni loading of 15 percent showed the best performance in terms of hydrogen production, and it also had the highest selectivity of hydrogen among the Ni/Al2O3 catalysts prepared by co-precipitation.

Bi-metallic or alloy metal catalysts have gained interest in ethanol steam reforming. Barroso et al. [20] synthesized NiZnAl catalysts using the citrate sol-gel method for ethanol reforming at temperatures ranging from 773-873 K. The product distribution was found to be highly dependent on the alloy composition, and with a Ni loading of 18-25 wt percent, a high hydrogen selectivity of approximately 85 percent was achieved. Kugai et al. [12] also investigated ethanol reforming using a CeO2-supported Ni-Rh bimetallic catalyst, but a dispersed Ni-Rh redox couple was observed instead of a NiRh alloy. The presence of Ni was found to improve Rh dispersion, while smaller CeO2 support-crystallite size improved Rh dispersion and resulted in strong Rh.CeO2 interaction.

Table 3
List of ethanol steam reforming over non-noble metal catalyst

Catalyst	Support	Temperature (K)	Steam/ethanol molar ratio	Ethanol conversion (%)
Ni (20 wt%)	La_2O_3	773	3:1	35
		1073		~ 100
	γ-Al_2O_3	973		77
		1073		100
Ni (20.6 wt%)	Y_2O_3	523	3:1	81.9
Ni (16.1 wt%)	γ-Al_2O_3			76
Ni (15.3 wt%)	La_2O_3			80.7
Ni (35 wt%)	γ-Al_2O_3	773	6:1	100
Ni (3.8 wt%)	Al_2O_3 (heat treatment at 823 K)	723	3:1	96.6
		923		100
	Al_2O_3 (heat treatment at 973 K)	723		100
		823		99.2
		923		100
Ni (10 wt%)	γ-Al_2O_3	923	8:1	100
	MgO			100
	La_2O_3			100
	ZnO			100
Co (10 wt%)	ZnO	623	4:1	100 (75 h)
Co (10 wt%), addition with Na				
Na (0.06 wt%)	ZnO	673	13:1	100
Na (0.23 wt%)				100
Na (0.78 wt.%)				100
Co (8 wt%)	Al_2O_3	673	3:1	74
(18 wt%)				99
(8 wt%)	SiO_2			89
(18 wt%)				97

Figure 4: List of ethanol steam reforming over non-noble metal catalyst [7].

4.3 Catalyst Preparation

A series of Ni-Co catalysts with varying compositions was prepared through co-precipitation method, utilizing a hydrotalcite (HT)-like material as the support. The total metal loading was set at 40 %. To prepare the cation solution, a mixture of Co(NO3)2 (29.12 g), Mg(NO3)2 6H2O (32.00 g), and Al(NO3)3 9H2O (28.14 g) was dissolved in 400 mL of deionized water and stirred. Simultaneously, the anion solution, containing NaOH (24 g) and Na2CO3 (5.962 g) in 400 mL of deionized water, was slowly added to the flask over a period of 2 hours. After the complete addition of the anion solution, the pH of the mixture was adjusted to 8-9 using nitric acid or NaOH, and the resulting mixture was heated to 80 degrees Celsius for 16 hours. Subsequently, the resulting precipitate was cooled, filtered, and washed thoroughly with deionized water. The catalyst was then dried under vacuum at 70 degrees Celsius overnight and calcined in flowing air at 600 degrees Celsius for 6 hours, with a heating rate of 5 degrees Celsius per minute.

4.4 Catalyst Characterization

X-ray diffraction

X-ray diffraction is a technique developed by Max von Laue that enables us to infer the structure of crystalline or quasi-crystalline materials by analyzing the diffraction patterns. When X-rays with wavelengths comparable to the dimensions of the crystal lattice interact with the material, diffraction can occur. The resulting diffraction angles are determined by the distances between the atoms in the crystal lattice. By comparing the diffraction pattern with a database, the crystal structure can be identified. The relationship between the diffraction angles and the crystal lattice spacing is described by the Bragg equation (equation 18).

$$\mathrm{n} \cdot \lambda = 2\,\mathrm{d} \cdot \sin\theta$$

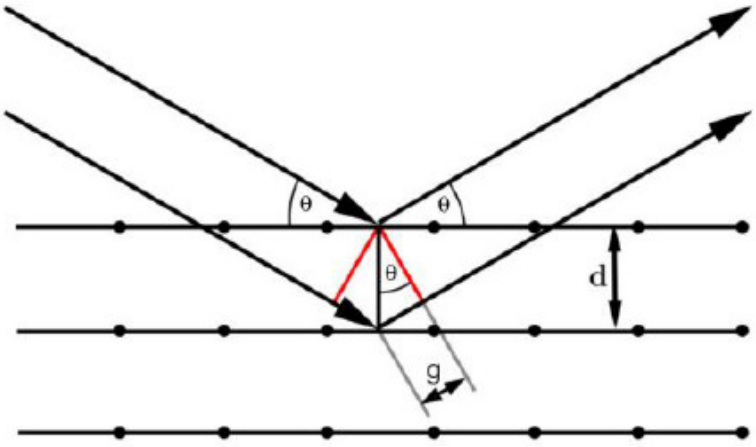

Figure 5: Schematic representation of the X-ray diffraction at the reticular plane. The g is the path difference [21].

Here lambda is the wavelength, theta is the angle to the lattice plane to the beam, d the distance of the lattice plane and n the degree of maximum in natural numbers N. Figure 5 represents these parameters schematically.

The X-ray diffraction patterns of the prepared HT precursors are presented in Fig. 6

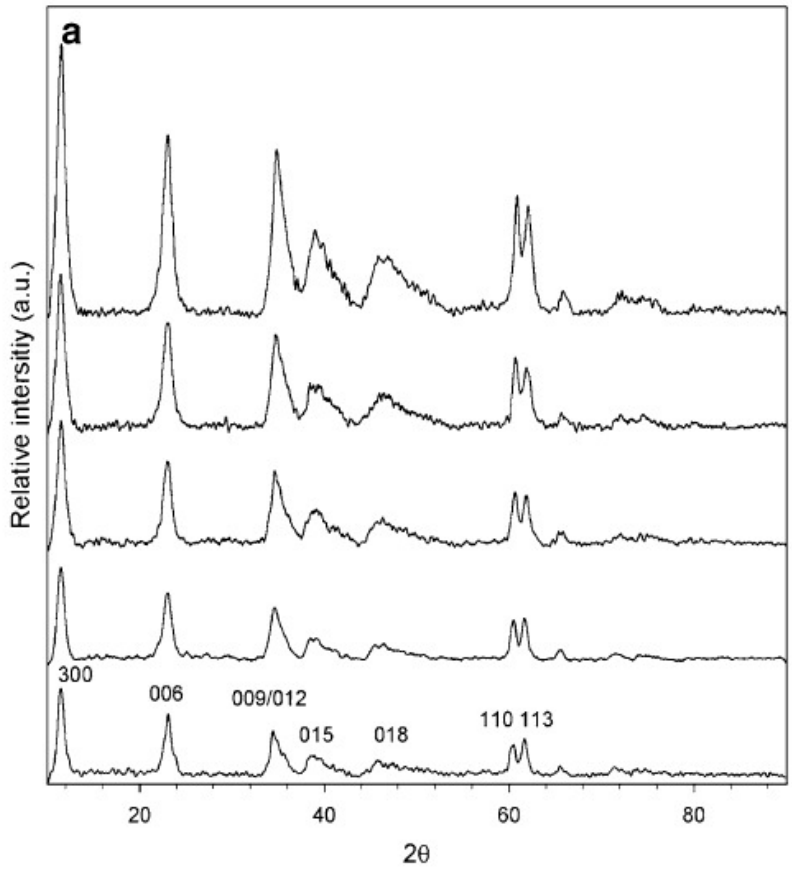

Figure 6: XRD patterns. From bottom: 40Co, 30Co–10Ni, 20Co–20Ni, 10Co–30Ni, 40Ni. a As prepared samples. b Calcined samples. Peaks marked with (O) are characteristic of Co3O4, CoAl2O4, NiAl2O4 [22].

The X-ray diffraction (XRD) analysis revealed the formation of characteristic diffraction reflections of the HT structure, while no spinel phases - typically observed as impurities in the preparation of HTs - were detected. The XRD patterns showed well-defined layered structures with sharp and symmetric peaks located at around 11, 22, and 35 degrees, corresponding to the (003), (006), and (009) crystal planes, respectively [23]. Broad and asymmetric peaks observed at approximately 35, 38, and 46 degrees were attributed to the (012), (015), and (018) crystal planes. The chemical composition of the samples showed a correlation with the XRD patterns, as an increase in Ni content led to an improvement in the degree of crystallinity, as indicated by the sharper XRD peaks. The incorporation of Ni+2 ions

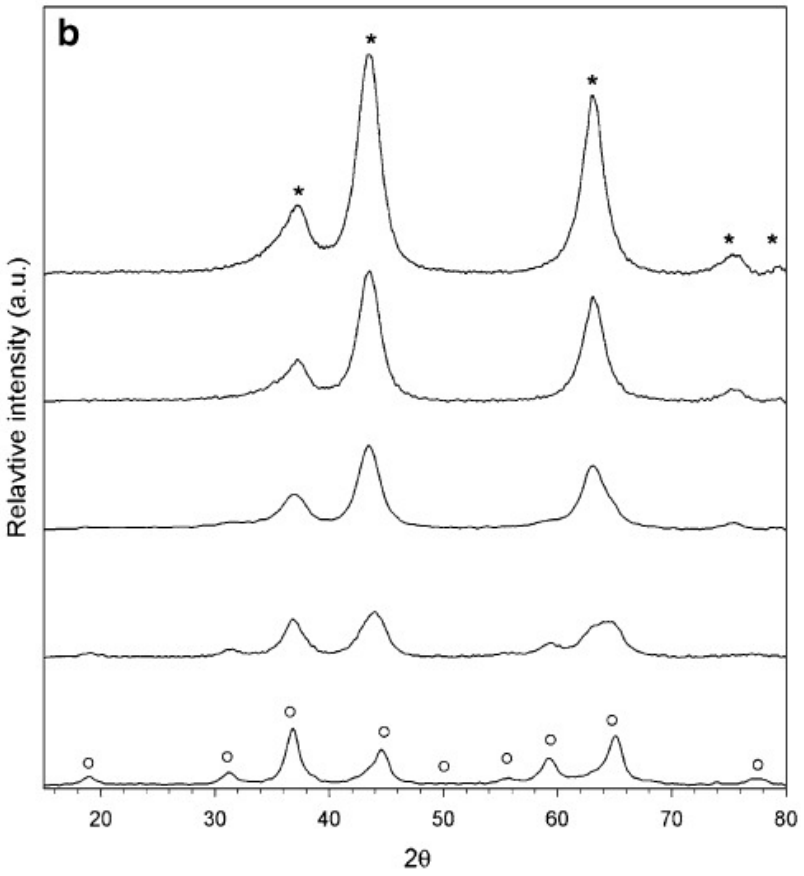

Figure 7: MgCo2O4, NiCo2O4, Al2 MgO4 and peaks marked with (*) are characteristic of NiO, MgNiO2 and MgO [22].

into the lattice of HTs was relatively easy due to its radius of 0.72, which is closer to the naturally occurring Mg+2 and Al+3 ions with radii of 0.65 and 0.60, respectively, compared to Co+2 ion radius of 0.74. Conversely, the relatively large Co+2 ions incorporated into the layers of HTs caused distortion of the HT structures, resulting in lower crystallinity. In summary, the XRD analysis provided evidence of the formation of a pure HT structure and demonstrated a correlation between the chemical composition and the degree of crystallinity [23].

Upon calcination at 600 degrees Celsius, the HT structure underwent a transformation into metal oxides, as evidenced by the XRD patterns illustrated in Figure 7. In the case of Co-based catalysts, the

XRD analysis did not identify single oxides CoO or Co2O3, indicating that Co+3/+2 ions were likely located in spinel-like structures such as CoAl2O4, Co2AlO4, MgCo2O4, NiCo2O4, and/or Co3O4. Since these oxides exhibit very similar characteristic XRD patterns [24], the obtained patterns of the catalysts in Figure 7 showed severe overlapping. The presence of peaks at 19 degrees suggested that Co3O4 and/or Co+3/+2 ions were incorporated into the alumina and magnesia spinel. Similar complexity was observed for NiO, where the overlapping reflections of NiO and MgNiO2 made it difficult to identify their phases. The peaks at 75.5 and 80 degrees were likely due to the formation of NiO and/or magnesium nickel oxide. Overall, it was challenging to determine whether Co3O4 and NiO formed a spinel together or were separately mixed in the solid solution of the matrix.

4.5 Thermal Analysis

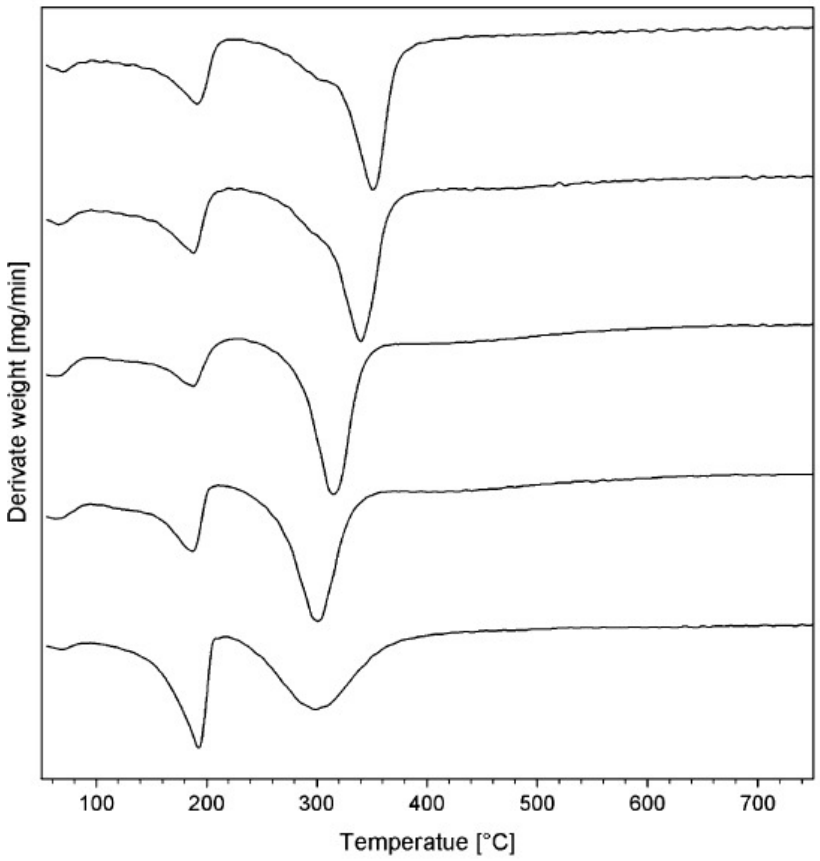

Figure 8: DTG curves for the as-prepared HT precursors. From bottom: 40Co, 30Co–10Ni, 20Co–20Ni, 10Co–30Ni, 40Ni [22].

Figure 8 shows the TG profiles of all the as-prepared HT precursors, illustrating the transformation of the HTs into the corresponding oxides during heating in air. In general, the clearly defined decomposition ranges are displayed for all the HTs and are consistent with the literature for these types of materials, providing complementary evidence to XRD for the formation of the HT structure [25].

The material under study undergoes weight loss in two distinct stages. The first stage, which occurs at temperatures ranging from 120 to 210 degrees Celsius, exhibits a maximum rate of weight loss at around 190 degrees Celsius. During this stage, interlayer and physisorbed water molecules are removed without disrupting the layered structure. In

the second stage, which takes place at temperatures above 210 degrees Celsius, hydroxyl groups are eliminated from the brucite-like layers, along with the removal of interlayer carbonate anions as CO2. This results in the loss of the layered structure and the transformation of the material into metal oxides. The transition temperature peaks at 299-350 degrees Celsius are relatively low when compared to the pure MgAlCO3-HTs, which have a reported temperature of 447 degrees Celsius. This suggests that the introduction of Ni+2 and/or Co+2 into Mg+2 sites destabilizes the HT structure. This observation is consistent with the XRD data, which indicate that the crystallinity of the HTs varies with the Ni–Co content due to differences in the ionic radii of Co+2 and Ni+2.

4.6 Physical–Chemical Properties

	BET			Chemisorption		
	Surface area uncalcined (m^2/g)	Surface area calcined (m^2/g)	Pore diameter calcined (nm)	D (%)	d (nm)	Metal surface area ($m^2_{metal}/g_{catalyst}$)
40Co/HT	73	103	14	6.5	15	17.6
30Co–10Ni/HT	92	106	16	6.5	15	17.5
20Co–20Ni/HT	94	141	6	8.7	11	23.3
10Co–30Ni/HT	120	180	7	11.3	9	30.2
40Ni/HT	144	153	9	13.9	7	36.9

Figure 9: Structural parameters of the HT-derived catalysts [22].

The BET surface areas and pore volumes of the prepared HT precursors and calcined catalysts are presented in Figure 9. The results for the 40Ni catalyst are consistent with those previously reported [26]. The as-prepared HT precursors exhibit BET surface areas ranging from 73 to 144 m2/g, with an average pore size of 6 to 16 nm, indicating that all of the catalysts are mesoporous materials. Upon calcination at 600 degrees Celsius, the catalysts show an increase in surface area, ranging from 103 to 180 m2/g. This finding is in agreement with Bellotto et al. [27], who observed that the surface area of HTs increases mainly due to the breakdown of the initial HT layer structure during the decomposition process.

To estimate the dispersion and particle size of the Ni–Co catalyst, chemisorption of hydrogen on the reduced catalyst was performed, and the results are shown in Figure 9. However, chemisorption studies of bimetallic Co-Ni catalysts are complex, and no standardized procedure is available. Typically, Ni is assumed to have near-zero activation energy of hydrogen adsorption, and a temperature of 300 K is commonly used for Ni hydrogen adsorption [28]. In contrast, a temperature of 400 K is recommended for Co due to the appreciable activation energy of hydrogen chemisorption on Co, which can result in a kinetic barrier at low temperature. Therefore, selecting the optimal experimental temperature can be challenging, as it affects the well-established monolayer adsorption on the Co-Ni surface. In our laboratory, separate experimental results have shown that the derivation of Co particle size at different temperatures can be significantly reduced by using the total uptake of hydrogen. In this study, the total hydrogen uptake was used to calculate dispersion and particle size, assuming that the HT-derived support material is generally considered unreduced under ambient conditions, and the physical adsorption of hydrogen on the support is negligible [29]. Based on the correlation between the results of chemisorption and XRD analysis, we conclude that the degree of formation of the HT-like structure is a crucial factor in determining the size of the metal particles.

4.7 Temperature Programmed Reduction

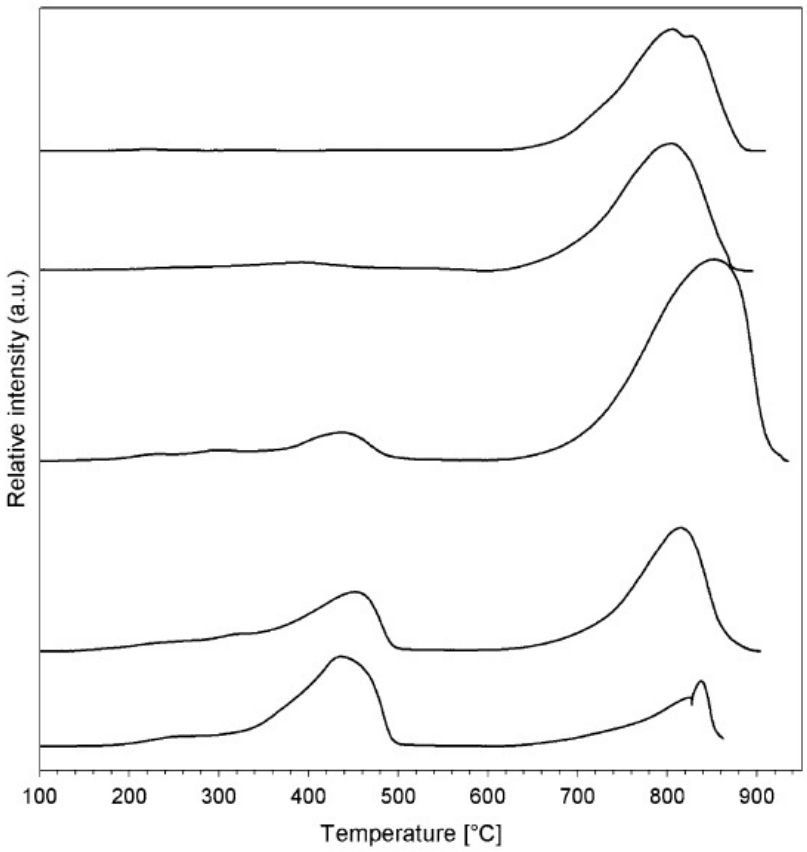

Figure 10: TPR profiles for the calcined HT samples. From bottom: 40Co, 30Co–10Ni, 20Co–20Ni, 10Co–30Ni, 40Ni [22].

Figure 10 displays the TPR profiles of the catalysts. The results indicate that the reducibility of the catalysts is highly dependent on their compositions: the Ni-rich catalysts exhibit greater resistance to reduction than the Co-rich catalysts, and the reducibility decreases in the following order: 40Co, 30Co–10Ni, 20Co–20Ni, 10Co–30Ni, and 40Ni catalysts.

The typical reduction order of pure Co and Ni oxides is contradicted in this study, where it was found that reduction from cobalt oxides to pure metal phase is easier than from nickel oxides. The interaction between the Co and Ni metals and the HT-derived supports explains this finding. Prior research has shown that the reducibility of Co and

Ni is affected by the initial degree of metal ion substitution into the HT lattice during preparation [30]. At the same metal loading, Co was reported to be less reducible than Ni in catalysts derived from co-precipitated HTs with similar crystallinity [31]. In this study, the 40Ni and 10Co-30Ni catalysts with close crystallinity showed similar reducibility and only one noticeable reduction range from 641 to 886 degrees Celsius, which is much higher than that observed for pure Ni and Co oxides. This is due to the strong interaction of Ni and Co with the support, and the reduction peak is typically associated with the extraction of Ni and Co atoms from the bulk solid solution to the surface. Additionally, as the Co loading increases, it becomes apparent that Co+2 ions are more challenging to substitute into the HT structures than Ni+2 ions. This affects the dispersion and diffusion of Co ions into the solid solution of Al2O3 and/or MgO, and only a fraction of the Co ions can be deeply incorporated within the HT derived matrix. Some of the Co ions tend to be expelled towards the surface, leading to differences in the extraction of Co ions from the HT-derived surroundings. Consequently, the reduction occurs in two temperature regions: 620 to 920 degrees Celsius and from 200 to 500 degrees Celsius. The peak areas at low temperature from 200 to 500 degrees Celsius increase with the Co content, and the 40Co catalyst exhibits the largest area.

4.8 STEM and EDS Mapping

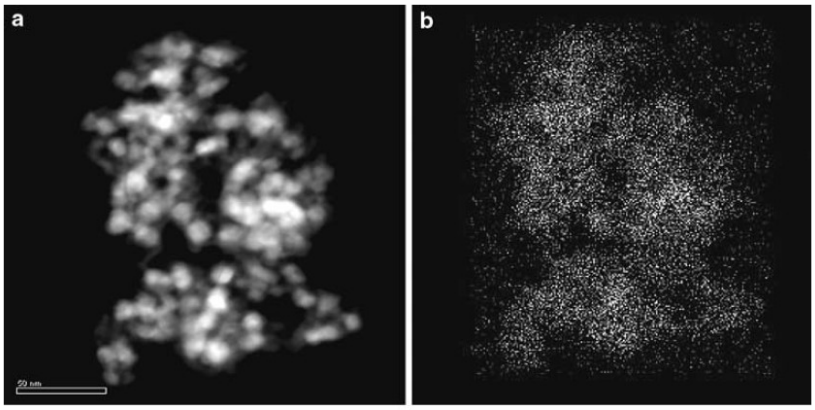

Figure 11: Dark field STEM micrograph and complementary mapping of the 30Co–10Ni catalyst (a), Al EDS mapping (b) [22].

The STEM evaluation of the reduced-passivated 30Co–10Ni catalyst revealed the presence of bright, roughly spherical particles containing Co+3/+2/0 and Ni+2/0 embedded in the surrounding MgO/Al2O3 matrix, as seen in Fig. 11a. The MgO/Al2O3 matrix appears grey due to lower atomic numbers compared to the Co/Ni particles. The distribution of the metals in the STEM image was confirmed by the EDS mapping of Al, Mg, O, Co, and Ni in the same field of view, as shown in Fig. 11b–12f. The Co and Ni particles showed the same morphology of distribution, indicating homogenous mixing of the two elements in the metal particles and the formation of an alloy. .

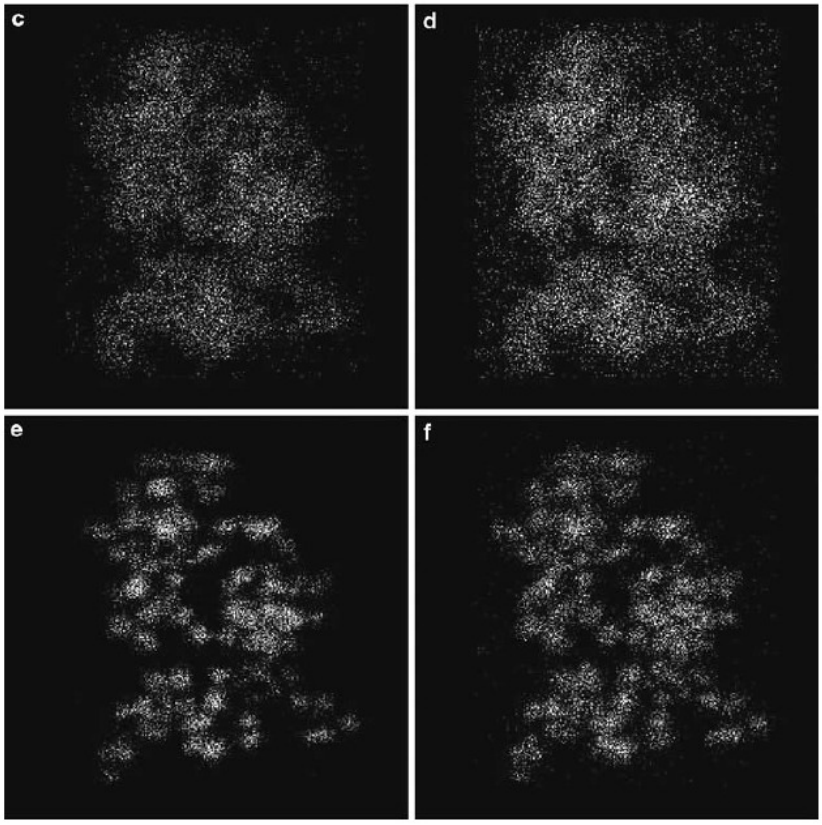

Figure 12: Mg EDS mapping (c), O EDS mapping (d), Co EDS mapping (e), and Ni EDS mapping (f) [22].

4.9 Catalyst Testing

The performance and durability of the catalysts were evaluated in an atmospheric pressure tubular fixed-bed steel reactor. To prepare the reactor, 10 mg of HT catalyst (250-500 µm) was mixed with 100 mg of a-Al2O3 and placed in a fixed-bed reactor with an inner diameter of 9.3 mm. Gases were delivered using Bronkhorst mass flow controllers, while a liquid flow controller was used to deliver a mixture of ethanol and water in a molar ratio of 1:6, which was then carried by an Ar flow of 25 mL/min, vaporized in an evaporator, and directed into the reactor, which was heated using an electric furnace. The reforming reaction was conducted at 575°C, with a liquid flow of 5.7 g/h and an N2 flow of 60 mL/min, which served as an internal standard. The contact time, designated as W/F, was calculated as the ratio of the mass of the catalyst in grams to the molar flow rate of the inlet ethanol.

The reactor effluent was directed into a water-cooled condenser, where high boiling point products were collected and the gas flow was analyzed using an online Agilent M3000 Micro GC equipped with a Plot U column, a Molsieve molecular sieve column, and a thermal conductivity detector. The liquid effluent was collected and analyzed using 1H NMR spectroscopy. Approximately 200 mg of the liquid was weighed, diluted by a factor of 20 with TMS/CDCl3 (0.05 percent v/v), dried with CaCl2, and transferred to a NORELL 507-HP NMR tube with a total volume of 700 µL. The 1H NMR measurement was conducted using a Bruker Avance DMX300 with a 5 mm QNP probe in a non-spinning mode at 25°C. The data acquisition involved a 90-degree excitation pulse, a sweep width of 16 ppm, a transmitter frequency offset of 6.0 ppm, a relaxation delay (d1) time of 4 s, a time domain data size of 64k, 64 scans, and 2 dummy scans. The quantification of the observed species was based on the integrals of the 1H peaks, specifically 1H (1.25 ppm) for ethanol and 1H (2.25 ppm) for acetaldehyde.

The product distribution was calculated by determining the water-free composition of the gas and liquid effluent, as well as the carbon mass balance. The fractions in the effluents were determined using the following formulas.

$$\text{Conversion of ethanol to syngas} = \frac{\text{moles of ethanol converted to syn gas}}{\text{moles of ethanol fed}} \cdot 100 \qquad (19)$$

$$\text{Conversion of ethanol to acetaldehyde} = \frac{\text{moles of ethanol converted to acetaldehyde}}{\text{the moles of ethanol fed}} \cdot 100 \qquad (20)$$

$$\text{Unreacted ethanol} = \frac{\text{the moles of ethanol fed} - \text{the moles of ethanol reacted}}{\text{the moles of ethanol fed}} \cdot 100 \qquad (21)$$

Here, syn gas includes H2, CH4, CO, CO2, C2H4 and C2H6. The H2 selectivity was defined as the following.

$$\text{H}_2\text{ selectivity} = \frac{\text{the number of hydrogen atoms in H}_2}{\text{the number of hydrogen atoms in syn gas and syn}-\text{gas intermediates}} \cdot 100 \qquad (22)$$

Based on the stoichiometric H2 production from ethanol in Eq. 1, the H2 yield was defined as:

$$\text{H}_2\text{yield} = \frac{\text{moles of H}_2\text{ produced}}{6.\text{ moles of ethanol fed}} \cdot 100 \qquad (23)$$

Turn over frequency (TOF) and deactivation function (U) were defined as:

$$\mathrm{TOF} = \frac{\text{the number of ethanol molecules converted to syn gas and syn}-\text{gas intermediates}}{\text{the number of catalyst atoms exposed on the surface}} \tag{24}$$

$$\mathrm{U} = \frac{\text{the activity of the catalyst on stream at the time}}{\text{the initial activity of the catalyst}} \tag{25}$$

4.10 Sintering

The loss of active site area in a catalyst is caused by the accumulation of smaller particles into larger ones, a process known as sintering. Several factors contribute to sintering, including reaction temperature, gas composition over the catalyst, catalyst structure and composition, and metal-support interactions. Among these factors, reaction temperature has been identified as the main cause of sintering. To prevent sintering, various techniques can be employed, such as suitable catalyst preparation methods that allow for the formation of metal particles with small sizes and high dispersion. Additionally, engineering the support-metal interaction is crucial to promote the segregation of metal and the strong interaction between them, which helps to stabilize the catalyst particles.

4.11 Promoter effect on Ni-Co bimetallic catalysts

Catalyst deactivation due to coke formation is primarily caused by the acidic sites on the support material, which facilitate the dehydration of ethanol into ethylene, a precursor for carbon deposition. To address this issue, different strategies have been investigated, such as using alkali metal basic supports to neutralize the acidity of the support material. Ongoing research is focused on developing effective techniques to minimize coke formation and enhance catalyst efficiency.

Previous investigations have demonstrated that Ni catalysts derived from hydrotalcite exhibit exceptional activity and stability in comparison to other reforming Ni catalysts. The desirable features of these catalysts include their small Ni particle size, excellent resistance to carbon deposition, and remarkable stability, which make them highly sought-after for diverse applications.

De Chen et al. [22] conducted a study at the Norwegian University of Science and Technology (NTNU) where a hydrotalcite (HT)-like material was utilized as a support for Ni-Co bimetallic catalysts. The study observed that this approach effectively eliminated the acidity of the support material, resulting in a decrease in coke formation during ethanol steam reforming.

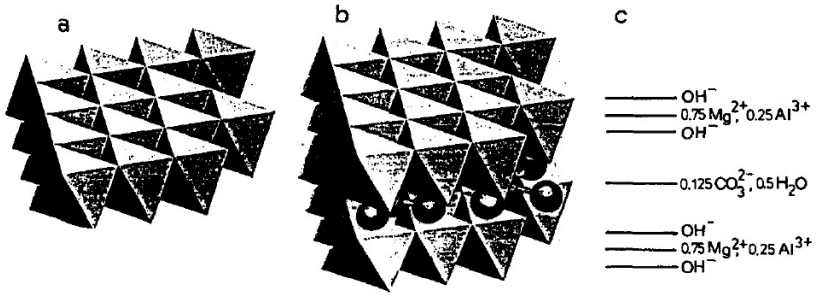

Figure 13: Brucite lattice (a), HTIc lattice (b), attom positions (c) [32].

The nomenclature of hydrotalcite is as follow:

$$\text{Hydrotalcite} = Mg_6Al_2(OH)_{16}CO_3 \cdot 4\,H_2O$$

Hydrotalcite (HT) is commonly composed of magnesium (Mg) and aluminum (Al). The structure of HT is derived from brucite, a magnesium hydroxide in which octahedral magnesium ions, coordinated to six hydroxyl groups, share edges to form infinite sheets. These sheets are stacked on top of each other and are held together by hydrogen bonding. When aluminum replaces some of the magnesium ions in brucite to form HT, a positive charge is created in the hydroxyl sheets. To counterbalance this positive charge, carbonate ions occupy the inter-layer region between two brucite sheets. The inter-layer region also contains water molecules, which occupy the free space [33].

5 Description of the installation

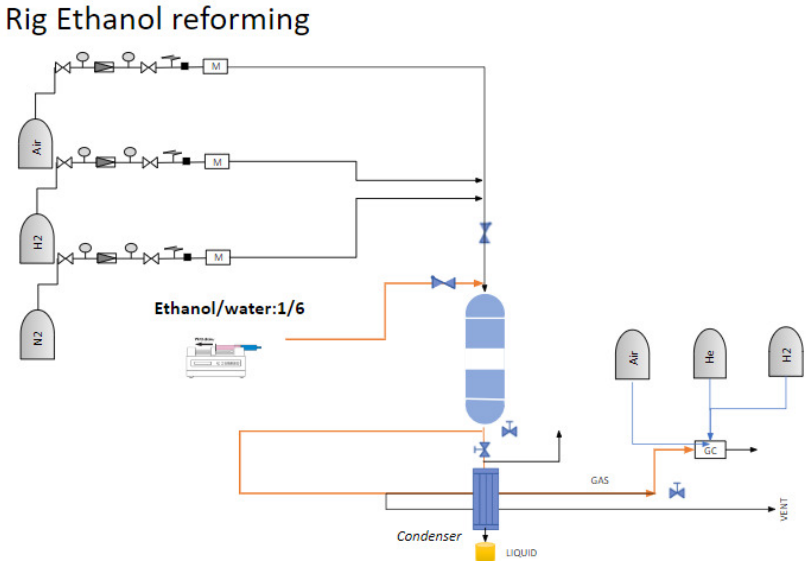

Figure 14: Schematic drawing of Ethanol Steam Reforming for Hydrogen Production Installation

The experiment on ethanol steam reforming was conducted using a dual fixed-bed reactor system operating at atmospheric pressure. A schematic illustration of the experimental set-up can be found in Figure 14.

Before conducting the experiments, the catalyst is reduced using hydrogen gas. During the experiment, a mixture of ethanol and water is fed into the reactor, where it is converted into a gaseous phase due to the high temperature. The resulting gaseous mixture passes through a condenser, where the heavier compounds are liquefied and removed from the system. The remaining gases, which are lighter, are then analyzed using gas chromatography (GC).

Nitrogen was introduced into the system as an inert gas to facilitate material balance calculations. In chemical processes, inert gases are commonly employed to ensure accurate determination of molar fractions and to maintain a constant total molar flow rate of reactants and products. By injecting nitrogen, the overall composition of the system remains unaffected while allowing for precise measurement of the various components involved in the reaction, including ethanol

and the reforming products. This approach enhances the reliability and accuracy of the material balance calculations conducted during the experiment.

In the context of ethanol steam reforming, the removal of water from the reaction system is crucial to prevent interference with the reaction equilibrium. To achieve efficient water removal, nitrogen was introduced as a carrier gas. As an inert gas, nitrogen helps to carry away the water vapor produced during the reaction, aiding in its effective removal from the installation. This step ensures that the presence of water does not adversely impact the reaction kinetics or equilibrium, thereby allowing for more reliable analysis of the reforming process and accurate determination of the reaction products.

6 Kinetic Theory

6.1 Conversion

The conversion in the ethanol steam reforming process refers to the extent to which ethanol is transformed into its reaction products, primarily hydrogen, carbon monoxide, carbon dioxide, and water. It is a crucial parameter that quantifies the efficiency of the reaction and provides insights into the reaction kinetics and performance of the catalyst.

The conversion is typically calculated by comparing the amount of ethanol consumed during the reaction to the initial amount of ethanol introduced into the system. This calculation can be expressed using the following equation:

$$\mathrm{X}=\frac{\mathrm{n}_{i,react}}{\mathrm{n}_{i,in}} \qquad (26)$$

With n as the change of moles with time of species i and X as conversion.

For this ethanol steam reforming experiments, conversion was calculated using the following equation.

$$\mathrm{X}=\frac{\mathrm{n(Sum\,of\,products\,containing\,carbon\,atoms)}}{\mathrm{n(Ethanol)}} \qquad (27)$$

The conversion value provides insights into the efficiency of the ethanol steam reforming process. A higher conversion indicates a greater extent of ethanol conversion to the desired products, primarily hydrogen. It reflects the effectiveness of the catalyst in promoting the desired reaction and the conditions employed in terms of temperature, pressure, and reactant concentrations.

Moreover, monitoring the conversion as a function of time or other variables allows for the determination of reaction kinetics. By comparing the conversion profiles at different reaction conditions, one can investigate the effects of temperature, pressure, catalyst composition, and other factors on the reaction rate and selectivity.

6.2 Reaction Rate

The reaction rate calculation is a fundamental aspect of studying the kinetics of the ethanol steam reforming process for hydrogen production. It allows us to quantify the speed at which the reactants undergo chemical transformations and provides valuable insights into the efficiency and performance of the catalyst.

Where W is the weight of the catalyst of 10mg which was used in most experiments and F(Ethanol) is the initial flow rate of ethanol, reaction rate V0 was calculated using the following equation.

$$V_0 = \frac{F_{Ethanol} \cdot X}{W} \qquad (28)$$

The initial flow rate of ethanol refers to the rate at which ethanol is introduced into the reaction system. It plays a crucial role in determining the availability of reactants and has a direct influence on the reaction kinetics. By considering the initial flow rate, we capture the contribution of ethanol to the reaction rate.

The conversion factor represents the extent to which ethanol is transformed into the desired reaction products, with hydrogen being the primary target. Expressed as a percentage, the conversion factor reflects the efficiency of the reaction. A higher conversion signifies a greater proportion of ethanol being converted to the desired products. By including the conversion in our formula, we account for the efficiency of the reaction and its impact on the reaction rate.

The weight of the catalyst is another crucial factor in the calculation. Catalysts provide an active surface for the reactants to interact, facilitating the desired chemical transformations. The weight of the catalyst directly influences the reaction rate by determining the catalyst's available surface area for reactant adsorption and subsequent product desorption. Normalizing the reaction rate by the weight of the catalyst allows for a meaningful comparison of catalyst performance.

By multiplying the initial flow rate of ethanol by the conversion factor and dividing the result by the weight of the catalyst, we obtain an estimation of the reaction rate, considering these important variables. This formula provides a simplified approach to assess the reaction rate in the ethanol steam reforming process.

It is essential to note that while this formula offers valuable insights, it represents a simplified estimation and may not capture all the complexities of the reaction kinetics. To enhance the accuracy and reliability of our findings, we supplemented this formula with rigorous experimental data, thorough analysis, and additional kinetic modeling techniques.

By including this scientific explanation and the corresponding formula in the kinetic theory section of our thesis, we provide a comprehensive understanding of the reaction rate calculation in the context of the ethanol steam reforming process. This contributes to our overall understanding of the kinetics and performance of the catalyst in hydrogen production.

6.3 Power Rate Law

The power rate law calculation is a fundamental aspect of studying the kinetics of the ethanol steam reforming process for hydrogen production. It enables us to determine the relationship between the reaction rate and the concentrations of the reactants involved. In the context of this process, the power rate law equation takes the form:

$$v_0 = k[A]^a[B]^b \qquad (29)$$

Where [A] and [B] express the reactant concentrations of the species A and B. The exponents a and b are the partial orders of reaction for A and B and the overall reaction order is the sum of the exponents. The constant K is the reaction rate constant of the reaction and its value depends on conditions such as temperature.

To determine the reaction orders and the rate constant, experimental data is collected by measuring the reaction rate at various concentrations of the reactants while keeping other conditions constant. The obtained data is then analyzed using mathematical techniques such as the method of initial rates or graphical analysis.

By plotting the experimental data and analyzing the relationship between the reaction rate and the concentrations of the reactants, it is possible to deduce the reaction orders (a and b) and the rate constant (k). The reaction orders indicate how the concentration of each reactant influences the reaction rate. A reaction order of 0 signifies no effect, while positive values indicate a positive influence, and negative values suggest an inhibitory effect.

The rate constant, k, represents the proportionality constant in the power rate law equation and accounts for factors such as temperature, pressure, and catalyst properties. It quantifies the intrinsic reactivity of the reaction and characterizes the efficiency of the catalyst.

The reaction rate and the concentrations of the reactants in the ethanol steam reforming process demonstrates the significance of experimental data analysis and the determination of reaction orders and rate constants in elucidating the kinetics of the reaction.

6.4 Turnover frequency (TOF)

In this study, turnover frequency (TOF) is defined as the number of molecules that react on each available catalytic site per unit time [34]. The surface-specific activities were calculated using the atomic rate and dispersion [35].

$$\mathrm{TOF}=\frac{\mathrm{Atomic\,rate}}{\mathrm{Dispersion}} \qquad (30)$$

Dispersion (D) is defined as the fraction of total atoms or molecules of the active phase available at the surface for catalysis.

During experiments, we substituted the rate v0 in power rate law equation with TOF so as to take into account the number of reaction products generated per active site per unit time. Therefore, the order of reaction was calculated using the following equation.

$$\mathrm{TOF}=\mathrm{k}[\mathrm{A}]^{a}[\mathrm{B}]^{b} \qquad (31)$$

6.5 Arrhenius Equation

The Arrhenius equation is a formula for the temperature dependence of reaction rates. This equation has a vast and important application in determining the rate of chemical reactions and for calculation of energy of activation.

The Arrhenius equation gives the dependence of the rate constant of a chemical reaction on the absolute temperature as.

$$\mathrm{k}=\mathrm{A}\cdot \mathrm{e}^{\frac{-\mathrm{E_a}}{\mathrm{RT}}} \qquad (32)$$

Where k is the rate constant, T is the absolute temperature, A is the pre-exponential factor, Ea is the activation energy and R is the universal gas constant.

The Activation Energy and pre-exponential factor was estimated from the graph plotted from the natural logarithm of the Arrhenius Equation which is as follows.

$$\ln k = \frac{-E_a}{R} \cdot \left(\frac{1}{T}\right) + \ln A \qquad (33)$$

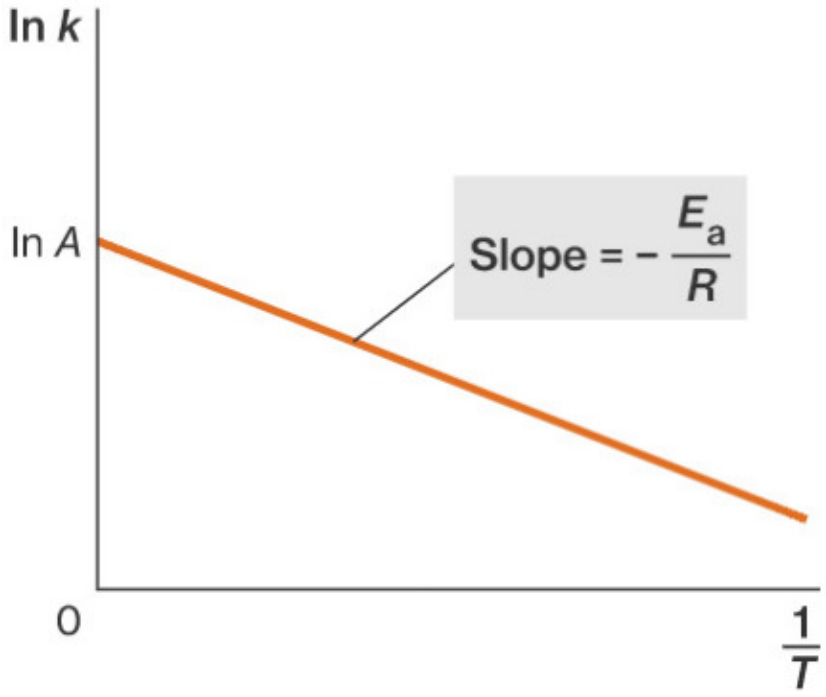

Figure 15: Graph of Arrhenius Equation [36].

7 Results and Discussion

In the following sections, the results of both 20Co20Ni and 35Co05Ni catalysts obtained will be described. In addition, the discussion of the attained results is going to be carried out trying to explain these results as well as basing them on the existing literature.

7.1 Transport limitations

7.1.1 Internal Transport Limitation

Internal mass transfer limitation refers to the challenges encountered in facilitating the diffusion of reactants and products within and out of the photo catalyst particle, as well as enabling light to penetrate the catalyst volume. This limitation arises due to the structure and characteristics of the catalyst, particularly in porous materials, and is influenced by its intrinsic properties [37].

30Co10Ni Catalyst size (micro m)	Catalyst mass (mg)	Temperature (degree celsius)	Ethanol/water Molar ratio	Ethanol/water Mixture Flow (micro l/min)	Nitrogen Flow (ml/min)
125-250	10	550	1/6	105	18.6
250-400	10	550	1/6	105	18.6

Figure 16: Internal transport limitation experimental procedure.

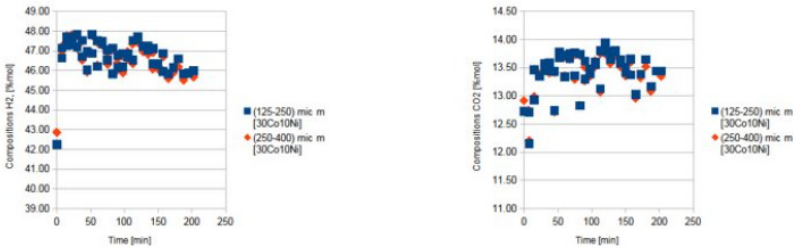

Figure 17: Results for internal transport limitation.

To determine whether there were internal transport limitations, we conducted experiments using catalysts of the same type but with varying sizes. From the results obtained, as shown in Figure 17, the difference in the compositions of hydrogen and carbon dioxide produced by the various sizes of the 35Co05Ni catalyst was found to be negligible. This suggests that there are no internal transport limitations.

7.1.2 External Transport Limitation

External transport limitations in a catalyst occur when factors outside the catalyst such as poor mixing, hinder the movement of reactant and product molecules. These factors make it difficult for molecules to reach the catalyst and participate in the reaction effectively.

35Co05Ni Catalyst (mg)	Temperature (degree celsius)	Ethanol/water Molar ratio	Ethanol/water Flow (micro l/min)	Nitrogen Flow (ml/min)
10	500	1/6	850	96
15	500	1/6	1275	96

Figure 18: External transport limitation experimental procedure.

35Co05Ni Catalyst (mg)	Ethanol/water Flow (Micro l/ min)	Rate constant (mol/ min*g*Pa)
10	850	$1*10^{-6}$
15	1275	$1*10^{-6}$

Figure 19: Results of external transport limitation experiment.

To investigate the possibility of external transport limitations, we conducted experiments using varying flow rates of the ethanol-water mixture and masses of the catalyst.

The rate constant obtained from two experiments carried out with different ethanol-water flow rates and catalyst masses was found to be similar. This suggests that there are no external transport limitations.

7.2 Ethanol Reaction Order

Ethanol steam reforming reaction is a complex set of chemical transformations, and it's crucial to determine the reaction kinetics to optimize the reaction conditions. In this study, we aimed to determine the order of reaction with respect to the ethanol concentration in the ethanol steam reforming process.

Temperature (degree celsius)	Nitrogen Flow (ml/min)	Ethanol/water mixture Flow (micro l/min)	Ethanol/water Molar ratio
550	96	800	**1/8**
550	96	800	**1/7**
550	96	800	**1/6**

Figure 20: Ethanol reaction order experimental procedure.

The ethanol steam reforming reaction was performed in a dual fixed-bed reactor system at a constant temperature of 823.3K. The reaction parameters were varied by changing the concentration of ethanol-water molar ratio while maintaining the other variables constant. The reactants were fed into the reactor and passed over a NiCo catalyst. The products were then analyzed using a gas chromatograph to obtain the concentrations of CO2, H2, CO etc.

7.2.1 Results for 20Co20Ni/HT catalyst

Conversion was calculated using the following equation

$$X = \frac{n_{i,react}}{n_{i,in}} \qquad (26)$$

Table 2
Comparison of Percentage Conversion of Ethanol at Various Ethanol-Water Molar Ratios

Ethanol : Water	% Conversion
1 : 8	21.88
1 : 7	22.33
1 : 6	22.52

The observed increase in conversion with a change in the ethanol to water ratio from 1:8 to 1:6 can be attributed to several factors (Table 2). One such factor is the water-gas shift reaction (Equation 11). In steam reforming, the presence of water facilitates the water-gas shift reactions alongside ethanol steam reforming. By reducing the ethanol to water ratio and increasing the water concentration, the water-gas shift reaction is promoted. This reaction converts carbon monoxide (CO) and water (H2O) into carbon dioxide (CO2) and hydrogen (H2). As a result, the overall hydrogen production is enhanced, leading to an increase in the conversion of ethanol to hydrogen.

The increased conversion can also be attributed to the higher water vapor content achieved by reducing the ethanol to water ratio. Water vapor plays a vital role in the steam reforming process as it assists in activating the catalyst and facilitating the necessary reaction steps. By increasing the water vapor content through a lower ethanol to water ratio, the contact between the reactants and the catalyst surface is improved. This improved contact enhances the efficiency of the catalyst in breaking down ethanol molecules and promoting the desired reforming reactions. Consequently, the conversion of ethanol to hydrogen is increased.

Furthermore, the change in the ethanol to water ratio can influence the reaction kinetics involved in ethanol steam reforming. Modifying the water content affects the rate-determining step(s) of the reaction. By altering the concentration of water, the energy barriers associated with specific reaction steps may be impacted, leading to a different rate-determining step. This change in the rate-determining step can result in an overall increase in the reaction rate and, consequently, in the conversion of ethanol to hydrogen.

Table 3
Product Quantities from Ethanol Steam Reforming (Ethanol-to-Water Molar Ratio: 1 to 8) Table 4

Products	% Quantity
Hydrogen	48
Carbon dioxide	13
Methane	2
Carbon monoxide	4
Nitrogen	33

Product Quantities from Ethanol Steam Reforming (Ethanol-to-Water Molar Ratio: 1 to 7) Table 5

Products	% Quantity
Hydrogen	48
Carbon dioxide	13
Methane	2
Carbon monoxide	4
Nitrogen	33

Product Quantities from Ethanol Steam Reforming (Ethanol-to-Water Molar Ratio: 1 to 6) Table 6

Products	% Quantity
Hydrogen	52
Carbon dioxide	14
Methane	2
Carbon monoxide	4
Nitrogen	28

The slight increase in the quantity of hydrogen produced by 4 percent after changing the ethanol to water ratio from 1:8 to 1:6 can be explained by several factors (Table 3-6). As mentioned earlier, the change in the ethanol to water ratio affects the concentration of water in the reaction mixture. With a lower ethanol to water ratio, the water concentration increases. This can promote the water-gas shift reaction (Equation 11), which converts carbon monoxide (CO) and water (H2O) into carbon dioxide (CO2) and hydrogen (H2). The increase in the water concentration by reducing the ethanol to water ratio provides more reactant molecules for the water-gas shift reaction, leading to a higher production of hydrogen.

Ethanol steam reforming is an equilibrium-based reaction, and the concentrations of reactants can influence the equilibrium position. By decreasing the ethanol to water ratio, the relative concentration of water in the reaction mixture increases. According to Le Chatelier's Principle, an increase in the concentration of one reactant (water, in this case) can drive the equilibrium towards the product side (hydrogen). This shift in the equilibrium position favors the forward reaction, resulting in a higher quantity of hydrogen produced.

The change in the ethanol to water ratio can impact the performance of the catalyst used in the ethanol steam reforming process. The presence of water vapor is known to enhance the catalytic activity and improve the efficiency of the catalyst. With a higher water vapor content achieved by reducing the ethanol to water ratio, the catalyst may exhibit improved performance in breaking down ethanol and promoting the desired reforming reactions. This enhanced catalyst activity can contribute to the increased production of hydrogen.

Where W is the weight of the catalyst of 10mg which was used in most experiments and F(Ethanol) is the initial flow rate of ethanol, reaction rate V0 was calculated using the following equation.

$$\mathrm{V_0}=\frac{\mathrm{F}_{Ethanol}\cdot \mathrm{X}}{\mathrm{W}} \qquad (28)$$

The estimation of the ethanol reaction order (x) was accomplished by employing a logarithmic equation to analyze the experimental data. The equation used can be expressed as:

$$\ln \mathrm{V_0}=\mathrm{n}\cdot \ln[\mathrm{Ethanol}]+\ln \mathrm{K} \qquad (34)$$

In this equation, 'rate' represents the observed reaction rate, '[Ethanol]' denotes the concentration of ethanol, and 'n' represents the reaction order with respect to ethanol. By taking the natural logarithm of the reaction rate and plotting it against the logarithm of the ethanol concentration, a linear relationship was expected if the reaction followed a specific order with respect to ethanol.

The utilization of a logarithmic transformation offers a more comprehensive interpretation of the data. If the plot resulted in a straight line with a slope of 'n', it would indicate that the reaction order with respect to ethanol is indeed 'n'. Deviations from linearity or a slope different from 'n' would suggest a different reaction order.

By fitting the experimental data to this logarithmic equation and analyzing the resulting plot, we were able to estimate the ethanol reaction order ('n') and gain insights into the kinetics of the ethanol steam reforming reaction.

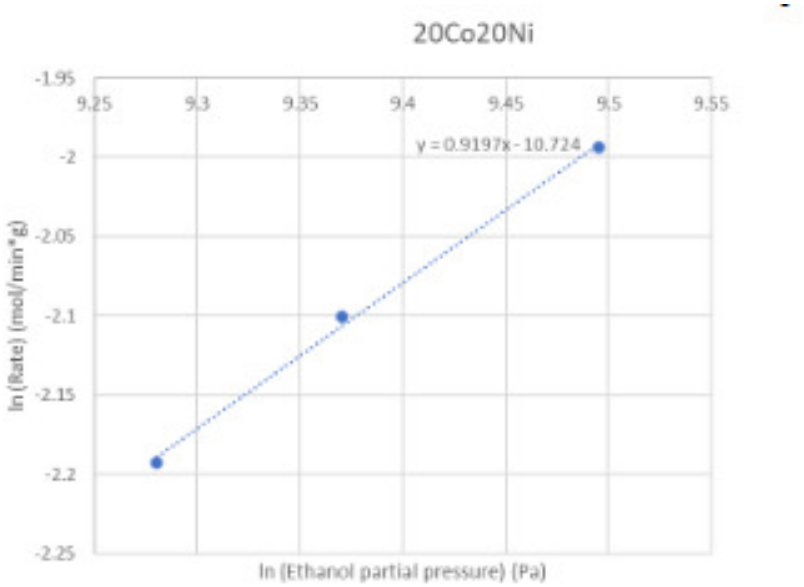

Figure 21: Ethanol reaction order for 20Co20Ni catalyst.

The results showed that the reaction is first-order with respect to ethanol concentration. This implies that doubling the ethanol concentration will double the rate of the reaction. Ethanol reaction order was found to be 0.9197 from the analysed experimental data.

7.2.2 Results for 35Co05Ni/HT catalyst

Conversion was calculated using the following equation

$$X = \frac{n_{i,react}}{n_{i,in}} \qquad (26)$$

Comparison of Percentage Conversion of Ethanol at Various Ethanol-Water Molar Ratios (Table 7)

Ethanol : Water	% Conversion
1 : 8	17.51
1 : 7	18.11
1 : 6	18.32

Product Quantities from Ethanol Steam Reforming (Ethanol-to-Water Molar Ratio: 1 to 8) Table 8

Products	% Quantity
Hydrogen	42
Carbon dioxide	10
Methane	1
Carbon monoxide	4
Nitrogen	43

Product Quantities from Ethanol Steam Reforming (Ethanol-to-Water Molar Ratio: 1 to 7) Table 9

Products	% Quantity
Hydrogen	44
Carbon dioxide	11
Methane	1
Carbon monoxide	4
Nitrogen	40

Product Quantities from Ethanol Steam Reforming (Ethanol-to-Water Molar Ratio: 1 to 6) Table 10

Products	% Quantity
Hydrogen	45
Carbon dioxide	11
Methane	2
Carbon monoxide	4
Nitrogen	38

The conversion increases with changes of Ethanol-Water Molar Ratios from 1 : 8 to 1 : 6 for 35Co05Ni/HT catalyst which is the similar trend observed for 20Co20Ni/HT catalyst (Table 7). Hydrogen quantity produced also increased slightly with changes of Ethanol-Water Molar Ratios from 1 : 8 to 1 : 6 for 35Co05Ni/HT catalyst which is the similar pattern observed for 20Co20Ni/HT catalyst (Table 8-10).

Where W is the weight of the catalyst of 10mg which was used in most experiments and F(Ethanol) is the initial flow rate of ethanol, reaction rate V0 was calculated using the following equation.

$$V_0 = \frac{F_{Ethanol} \cdot X}{W} \qquad (28)$$

The estimation of the ethanol reaction order (n) was accomplished by employing a logarithmic equation to analyze the experimental data. The equation used can be expressed as:

$$\ln V_0 = n \cdot \ln[\text{Ethanol}] + \ln K \qquad (34)$$

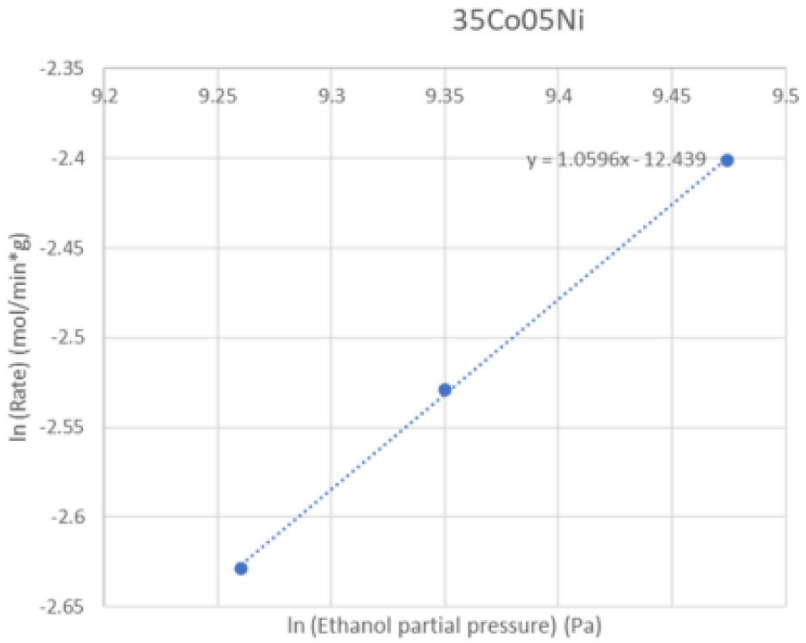

Figure 22: Ethanol reaction order for 35Co05Ni catalyst.

The results for 35Co05Ni catalyst indicate first order reaction which is similar to 20Co20Ni catalyst. Ethanol reaction order was found to be 1.0596 from the analysed experimental data.

7.2.3 Conclusion

Catalyst	Ethanol reaction order
35Co05Ni	1.06
20Co20Ni	0.92

Figure 23: Ethanol reaction order.

NB-It is important to highlight that nitrogen is generally considered inert due to its stable molecular structure and limited reactivity under typical conditions. While nitrogen may exhibit some reactivity under specific circumstances, such as at high temperatures or in the presence of certain catalysts, the conditions and catalysts employed in this ethanol steam reforming experiment do not promote nitrogen reactivity. Therefore, the inclusion of nitrogen as an inert gas does not significantly interfere with the reaction itself, ensuring the validity and reliability of the experimental results obtained.

Two catalysts, namely 20Co20Ni and 35Co05Ni, were compared in terms of their catalytic activity. The study found that the ethanol steam reforming reaction is first-order with respect to ethanol concentration as observed from both catalysts. The 20Co20Ni catalyst exhibited higher conversion of ethanol and produced a greater quantity of hydrogen compared to the 35Co05Ni catalyst.

The composition of a catalyst plays a crucial role in determining its catalytic activity. In this case, the 20Co20Ni catalyst contained equal amounts of cobalt (Co) and nickel (Ni), while the 35Co05Ni catalyst had higher cobalt content and lower nickel content. This difference in composition likely contributed to the variation in catalytic performance observed. The specific composition of the catalyst can influence the formation and accessibility of active sites, where reactant molecules can adsorb and undergo chemical reactions. The 20Co20Ni catalyst may have had a higher concentration of active sites favorable for ethanol steam reforming, resulting in enhanced conversion and hydrogen production.

The combination of cobalt and nickel in the catalysts may have also contributed to synergistic effects, where the presence of both elements enhances the overall catalytic activity. The specific ratio of

cobalt to nickel in the 20Co20Ni catalyst could have promoted synergistic interactions, resulting in superior performance compared to the 35Co05Ni catalyst.

7.3 Hydrogen Reaction Order

In this experiment, we investigated the effect of hydrogen concentration (or partial pressure) on the rate of the ethanol steam reforming reaction. The primary objective was to determine the impact of varying hydrogen flow rates on the reaction rate and gain insights into the kinetics of the ethanol steam reforming process.

Temperature (degree celsius)	Ethanol/water mixture Flow (micro l/ min)	Ethanol/water Molar ratio	Hydrogen Flow (ml/min)	Nitrogen Flow (ml/min)	Total gas Flow (ml/min)
550	850	1/6	0	96	96
550	850	1/6	15	81	96
550	850	1/6	25	71	96
550	850	1/6	35	61	96
550	850	1/6	45	51	96
550	850	1/6	65	31	96

Figure 24: Hydrogen reaction order experimental procedure.

The experiment was conducted under constant temperature, ethanol-water mixture flow, and molar ratio conditions. The flow of hydrogen was varied from 0 to 65 ml/min in order to determine the effect of hydrogen on the rate of reaction. The hydrogen partial pressure and rate of reaction were measured and recorded for each flow rate. The rate of reaction was calculated as the rate of ethanol consumption.

One limitation of this study is that it was conducted under constant temperature, ethanol-water mixture flow, and molar ratio conditions. In a real-world situation, these conditions are likely to vary, which could affect the order of reaction with respect to hydrogen.

7.3.1 Results for 20Co20Ni/HT catalyst

Conversion was calculated using the following equation

$$X = \frac{n_{i,react}}{n_{i,in}} \qquad (26)$$

Table 11
Comparison of Percentage Conversion at Various Hydrogen Flow Rate

Hydrogen Flow (ml/min)	% Conversion
0	27
15	22
25	20
35	18.7
45	16.8
65	15

The observed decrease in conversion with increasing hydrogen flow during ethanol steam reforming can be attributed to various factors (Table 11). One of the primary factors is competitive adsorption. In this reaction, both hydrogen and ethanol molecules are typically adsorbed onto the catalyst surface before undergoing the desired reforming reaction. As the hydrogen flow increases, the concentration of hydrogen molecules in the system rises. This leads to intensified competition between hydrogen and ethanol for available adsorption sites on the catalyst. Consequently, a greater number of hydrogen molecules may occupy the active sites, thereby reducing the number of active sites available for ethanol adsorption. As a result, the conversion of ethanol to the desired products decreases.

Another contributing factor to the decreasing conversion can be explained by Le Chatelier's Principle. Ethanol steam reforming is an equilibrium-based reaction. According to Le Chatelier's Principle, when the concentration of one of the reactants, such as hydrogen, is increased, the equilibrium position tends to shift in the direction that consumes or reduces the concentration of the excess reactant. In the case of ethanol steam reforming, an increase in hydrogen flow can lead to an excess of hydrogen molecules in the system. Consequently, the equilibrium of the reaction shifts in the reverse direction, favoring the reactant side. This shift results in a decrease in the conversion of ethanol, as a higher concentration of hydrogen opposes the desired forward reaction.

Additionally, the complex reaction kinetics involved in ethanol steam reforming can contribute to the observed decrease in conversion with increasing hydrogen flow. The reaction proceeds through a network of multiple reaction steps, and the rate-determining step(s) may be influenced by the concentration of hydrogen. At higher hydrogen flows, it is possible that the rate-determining step(s) become less favorable or exhibit a lower reaction rate. This change in the rate-determining step(s) can result in an overall decrease in the reaction rate, leading to a decrease in ethanol conversion.

Where W is the weight of the catalyst of 10mg which was used in most experiments and F(Ethanol) is the initial flow rate of ethanol, reaction rate V0 was calculated using the following equation.

$$\mathrm{V_0}=\frac{\mathrm{F}_{Ethanol}\cdot \mathrm{X}}{\mathrm{W}} \qquad (28)$$

In order to estimate the reaction order with respect to hydrogen, a logarithmic equation was employed to analyze the experimental data. The equation used was of the form:

$$\ln \mathrm{V_0}=\mathrm{n}\cdot \ln[\mathrm{Hydrogen}]+\ln \mathrm{K} \qquad (34)$$

In this equation, 'rate' represents the observed reaction rate, '[Hydrogen]' denotes the concentration or partial pressure of hydrogen, and 'n' represents the reaction order with respect to hydrogen. By taking the natural logarithm of the rate and plotting it against the logarithm of the hydrogen concentration, a linear relationship was expected if the reaction followed a specific order with respect to hydrogen.

The logarithmic transformation allows for a more straightforward interpretation of the data. If the plot resulted in a straight line with a slope of 'n,' it would suggest that the reaction order with respect to hydrogen is indeed 'n.' Deviations from linearity or a slope different from 'n' would indicate a different reaction order.

By fitting the experimental data to this logarithmic equation and analyzing the resulting plot, we were able to estimate the hydrogen reaction order ('n') and gain insights into the kinetics of the ethanol steam reforming reaction.

The reaction order with respect to 20Co20Ni catalyst is -1.74 due to the mechanism of ethanol reforming which is designed to examine the ethanol decomposition pathways which leads to various possible routes [38].

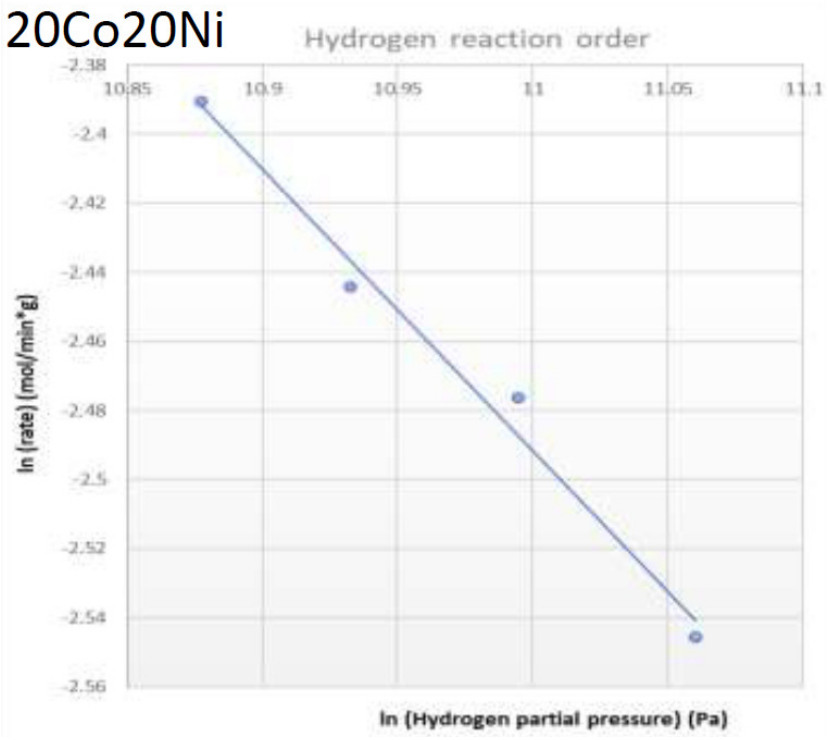

Figure 25: Hydrogen reaction order for 20Co20Ni catalyst.

7.3.2 Results for 35Co05Ni/HT catalyst

Conversion was calculated using the following equation

$$X = \frac{n_{i,react}}{n_{i,in}} \qquad (26)$$

Table 12
Comparison of Percentage Conversion at Various Hydrogen Flow Rate

Hydrogen Flow (ml/min)	% Conversion
0	19.45
15	17.88
25	16.87
35	16.60
45	14.81
65	14.29

There is decrease in conversion with increase in hydrogen flow for 35Co05Ni/HT catalyst which is also observed for the previous 20Co20Ni/HT catalyst (Table 12).

Where W is the weight of the catalyst of 10mg which was used in most experiments and F(Ethanol) is the initial flow rate of ethanol, reaction rate V0 was calculated using the following equation.

$$v_0 = \frac{F_{Ethanol} \cdot X}{W} \qquad (28)$$

In order to estimate the reaction order with respect to hydrogen, a logarithmic equation was employed to analyze the experimental data. The equation used was of the form:

$$\ln V_0 = n \cdot \ln[\text{Hydrogen}] + \ln K \qquad (34)$$

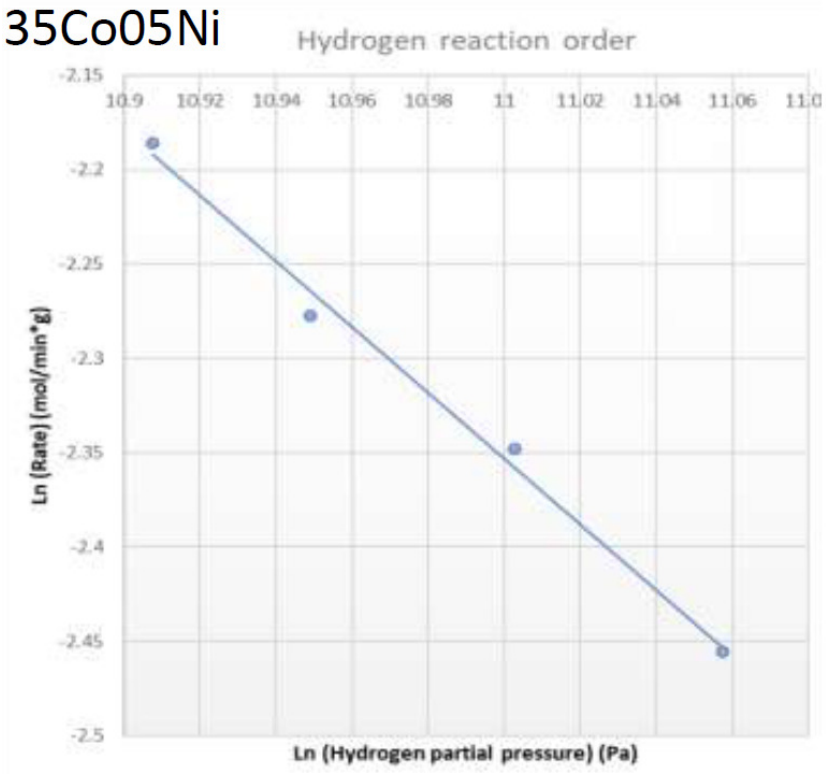

Figure 26: Hydrogen reaction order for 35Co05Ni catalyst.

The reaction order was -0.81 with respect to hydrogen. One possible explanation for such behavior is that the reaction pathway leading to the formation of hydrogen as a product is sensitive to the concentration of the ethanol reactant. For example, if the reaction pathway leading to hydrogen production involves an intermediate reaction step that is highly dependent on the availability of another reactant, then a decrease in the concentration of that reactant may reduce the rate of hydrogen production. Similarly, an increase in the concentration of that ethanol reactant may lead to greater competition for available reaction sites or slow down the reaction rate due to interactions between the different ethanol reactants.

7.3.3 Conclusion

A negative reaction order indicates an inverse relationship between the concentration of the reactant (in this case, hydrogen) and the reaction rate. So, as the hydrogen concentration increases, the reaction rate decreases. The magnitude of the negative reaction order indicates the extent to which the reaction rate is affected by changes in the hydrogen concentration.

For the 20Co20Ni catalyst, which has a reaction order of -1.74, the reaction rate decreases more significantly as the hydrogen concentration increases compared to the 35Co05Ni catalyst with a reaction order of -0.81. This means that even small increases in hydrogen concentration result in a larger decrease in the reaction rate for the 20Co20Ni catalyst.

The higher sensitivity of the 20Co20Ni catalyst to changes in hydrogen concentration suggests that the active sites on the catalyst surface, where the reaction takes place, are more influenced by the presence of hydrogen. It could be due to the specific composition and structure of the 20Co20Ni catalyst, which might have a higher affinity for hydrogen or a more complex surface chemistry that results in stronger interactions with hydrogen molecules.

On the other hand, the 35Co05Ni catalyst appears to be less sensitive to changes in hydrogen concentration, as indicated by its less negative reaction order. This suggests that the reaction rate for this catalyst is less affected by variations in the hydrogen concentration, indicating a different surface behavior and potentially different active sites.

7.4 Activation Energy

We investigated the activation energy of 35Co05Ni and 20Co20Ni catalysts for ethanol steam reforming by conducting experiments at three different temperatures (450, 500, and 550°C). The findings of this study provide important information for the development of new catalysts for ethanol steam reforming.

Temperature (°C)	Ethanol/water mixture flow (micro l/min)	Ethanol / water molar ratio	Nitrogen Flow (ml/min)
450	850	1/6	96
500	850	1/6	96
550	850	1/6	96

Figure 27: Activation energy experimental procedure.

In this study, we compare the activation energy of two catalysts for ethanol steam reforming in order to determine which catalyst is more effective. We conducted experiments at three different temperatures and analyzed the resulting data to gain insights into the catalytic performance of each catalyst.

In order to investigate the catalytic activity of the 35Co05Ni catalyst and the 20Co20Ni catalyst, we employed the Arrhenius equation, a fundamental tool in chemical kinetics, to estimate their respective activation energies. The Arrhenius equation establishes a relationship between the rate constant of a reaction, the temperature, and the activation energy.

Conversion was calculated using the following equation

$$\mathrm{X}=\frac{\mathrm{n}_{i,react}}{\mathrm{n}_{i,in}} \qquad (26)$$

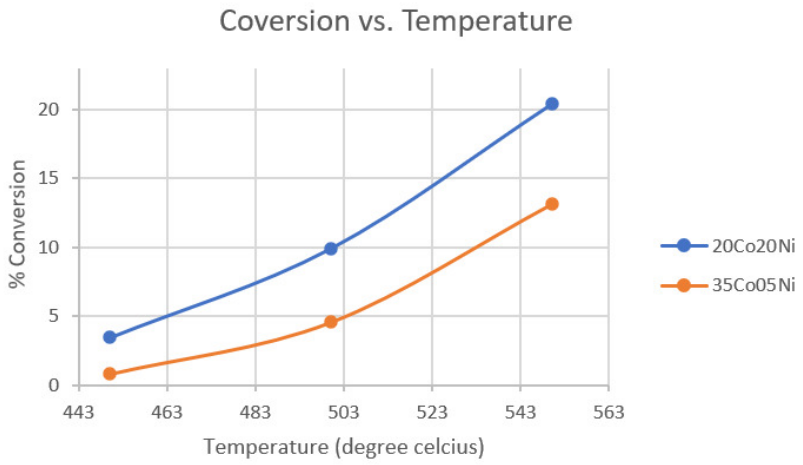

Figure 28

This behavior can be attributed to several factors. Firstly, the increased temperature enhances the kinetic energy of the reactant molecules, resulting in more frequent and energetic collisions. This heightened collision rate promotes a higher reaction rate, facilitating the conversion of ethanol to hydrogen and other desired products. The elevated temperature provides the necessary energy to overcome the activation energy barrier, enabling the reaction to proceed at an accelerated rate.

Additionally, the improved mass transfer at higher temperatures contributes to the observed increase in conversion. The increased thermal energy facilitates the diffusion of reactant molecules to the catalyst surface, enhancing the contact between the reactants and the active sites. This improved mass transfer allows for a greater number of reactant molecules to interact with the catalyst, thereby facilitating the reaction and leading to increased conversion.

Moreover, the thermodynamic equilibrium of the ethanol steam reforming reaction also plays a role. The elevated temperature induces a shift in the equilibrium towards the products, favoring the formation of hydrogen and other desired reaction products. This thermodynamic shift, coupled with the kinetic enhancements discussed earlier, contributes to the overall increase in conversion.

To estimate the activation energy for each catalyst, we utilized linear regression analysis. The Arrhenius equation, when expressed in the

form of a linear equation, is given by:

$$\ln k = \frac{-E_a}{R} \cdot \left(\frac{1}{T}\right) + \ln A \qquad (33)$$

In this equation, 'k' represents the rate constant, 'Ea' denotes the activation energy, 'R' is the gas constant, 'T' represents the absolute temperature, and 'A' is the pre-exponential factor. By taking the natural logarithm of the rate constant and plotting it against the inverse of the absolute temperature, a linear relationship was expected to emerge.

We performed linear regression analysis on the experimental data to obtain the slope and intercept of the resulting line. The slope of the line corresponds to the ratio of (-Ea/R), while the intercept represents the natural logarithm of the pre-exponential factor (ln(A)). Using this information, we calculated the activation energy for each catalyst by multiplying the slope by the gas constant (R).

The estimation of the activation energy provides valuable insights into the energetics of the catalytic reactions occurring on the surface of the catalysts. A higher activation energy suggests a greater energy barrier for the reaction and may indicate stronger chemical bonds or more complex reaction pathways. Conversely, a lower activation energy indicates a relatively easier reaction process.

By comparing the activation energies obtained for the 35Co05Ni catalyst and the 20Co20Ni catalyst, we can gain a deeper understanding of their respective catalytic performances. These results contribute to elucidating the effects of catalyst composition on the reaction kinetics and can aid in the optimization of catalyst design for desired reactions.

Results

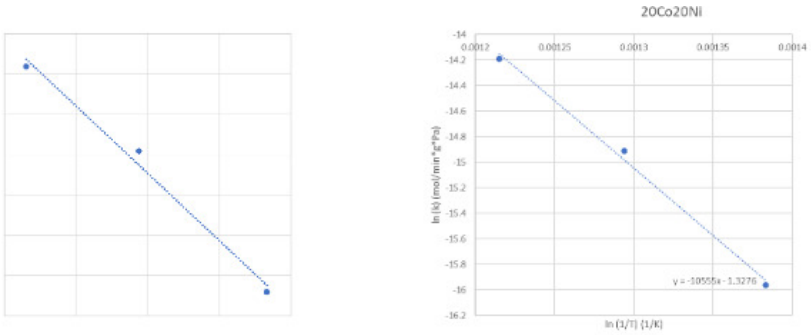

Figure 29: The graph to the left shows the results for 35Co05Ni catalyst and the one to the right shows the results for 20Co20Ni catalyst. These graphs were used to determine activation energies for both catalysts.

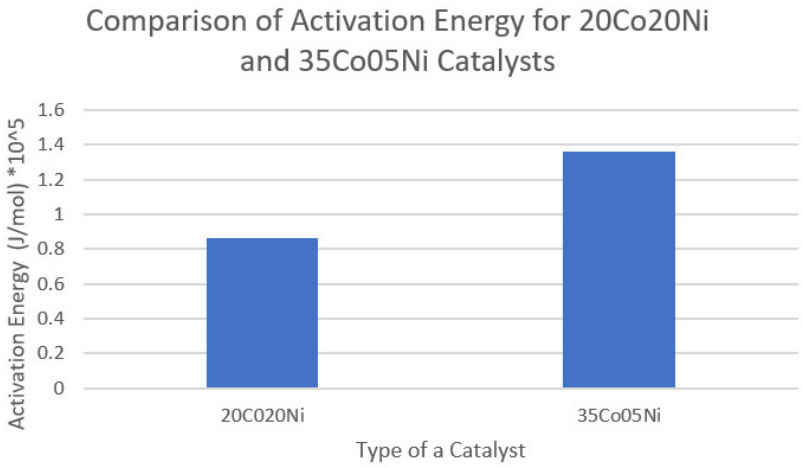

Figure 30

The results showed that 20Co20Ni Catalyst has a lower activation energy than 35Co05Ni Catalyst (Figure 28). 20Co20Ni Catalyst had an activation energy of 85.9 kJ/mol, while 35Co05Ni Catalyst had an activation energy of 135.9 kJ/mol. These results indicate that 20Co20Ni Catalyst is more efficient than 35Co05Ni Catalyst for ethanol steam reforming.

7.4.1 Conclusion

The 20Co20Ni catalyst has an activation energy of 85.9 kJ/mol, while the 35Co05Ni catalyst has an activation energy of 135.9 kJ/mol. This means that the 20Co20Ni catalyst requires less energy to initiate the ethanol steam reforming reaction compared to the 35Co05Ni catalyst.

A lower activation energy suggests that the 20Co20Ni catalyst provides more favorable reaction pathways or has more efficient active sites for the ethanol steam reforming reaction. It implies that the catalyst promotes the breaking of chemical bonds in ethanol and facilitates the production of hydrogen with less energy input.

The higher activation energy for the 35Co05Ni catalyst indicates that it has a higher energy barrier for the reaction to occur. This could imply that the catalyst is less efficient or less effective in promoting the desired reactions, resulting in a slower reaction rate or requiring more energy input.

8 Results Confirmation

Parameter	35Co05Ni	20Co20Ni
E_{a1} (J/mol)	1.36 E+5	0.86 E+5
T range (K)	723-873	723-873
Ethanol order	1.06	0.92

Figure 31: Results from my experiments.

Estimated kinetic parameters according to different authors

Parameter	This work	Other authors			
		Morgenstern et al.	Sun et al.	Akande et al.	Vaidya et al.
E_{a1} (J/mol)	2.07E+5	1.49E+5	1.87E+3–16.88E+3	4.41E+3	9.6E+4
E_{a2} (J/mol)	1.44E+5				
T range (K)	823–923	523–573	≈403	593–793	873–973
Ethanol order	0.75–0.8	1	0.43	1	1

Figure 32: Results of Ethanol Steam Reforming from previous researchers [39].

The results of my experimental study on the activation energy and the reaction order have been compared with those of previous researchers who conducted similar studies (Figure 30), and the results are found to be approximately similar . My study supports the findings of the previous work, which has contributed to the knowledge base of this field of research.

The activation energy values obtained for catalysts 35Co05Ni and 20Co20Ni in my study were within the range reported in previous studies. Also, the reaction order values were consistent with those of prior research. These similarities imply that my experimental design and procedures were reliable and that my results can be trusted, lending credibility to the study's overall findings.

9 Deactivation of Nickel-based catalyst

One of the primary challenges associated with using Nickel-based catalysts for ethanol steam reforming is the deposition of carbon resulting from various side reactions.

Reactions which contribute to carbon deposition on Nickel-based catalysts for ethanol steam reforming are: (i) Formation of ethylene from dehydration of ethanol (Equation(1)), ethylene is reduced to carbon species which are then deposited on the catalyst (Equation(2)), (ii) Decomposition of methane (Equation(14)), (iii) Boudouard reaction (Equation (15)).

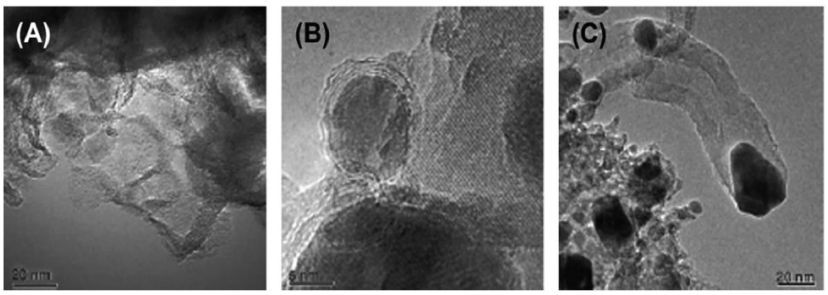

Figure 33: TEM images of different types of carbon formed over a Ni-based catalyst (A) amorphous, (B) encapsulating, and (C) filamentous carbon [40].

The deposition of carbonaceous materials during ethanol steam reforming can result in amorphous, filamentous, or encapsulating carbon on Nickel-based catalysts. Amorphous carbon usually forms at lower temperatures, typically between 200-250 degrees Celsius, while filamentous carbon is preferred at higher temperatures. Encapsulating carbon is thought to develop when carbon materials diffuse into the Nickel catalyst, resulting in the formation of nickel carbide (Ni-C).

It should be noted that the process of carbon deposition is continuous on the Nickel-based catalyst until the carbon content reaches a high enough level to push the Ni off the surface of the support. This results in the formation of carbon nanotubes (CNTs) and/or carbon nanofibers (CNFs), as shown in Figure 16.

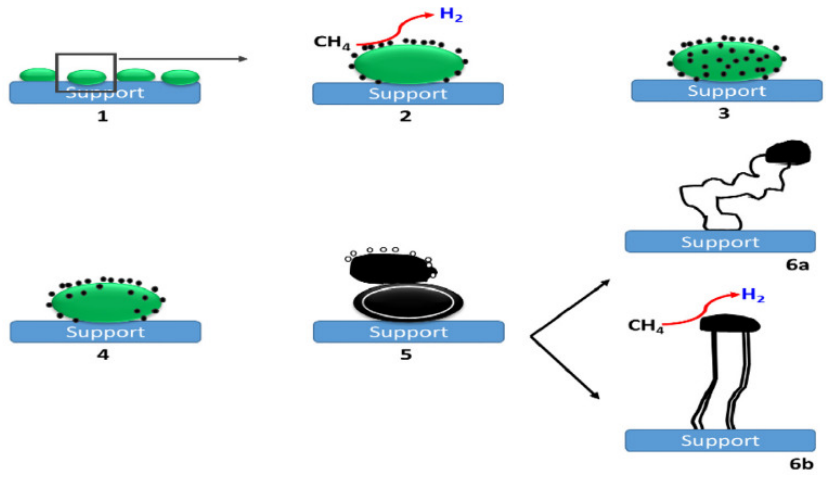

Figure 34: The mechanism for the formation of CNTs and CNFs over a supported catalyst [41].

The formation of carbon nanotubes (CNTs) and carbon nanofibers (CNFs) begins with nucleation, the initial stage in which carbon atoms diffuse across the interface between the catalyst and support. For CNFs, this diffusion occurs across the entire interface, resulting in the formation of complete fibers at low temperatures when the nucleation rate is slow. In contrast, CNT nucleation is limited to the vicinity of the gas-metal interface and is promoted by high temperatures.

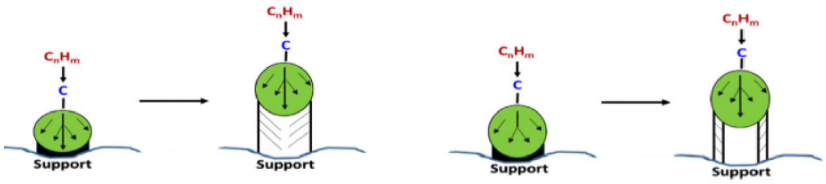

Figure 35: The formation of CNFs (left) and CNTs (right) [42].

As carbon layers deposit on the metal catalyst surface, encapsulating carbon is formed, leading to catalyst deactivation. However, the formation of filamentous carbon allows the catalyst to remain on top of the filament, accessible to reactants and intermediates, thus maintaining its activity during reforming reactions. This process is illustrated in Figure 18.

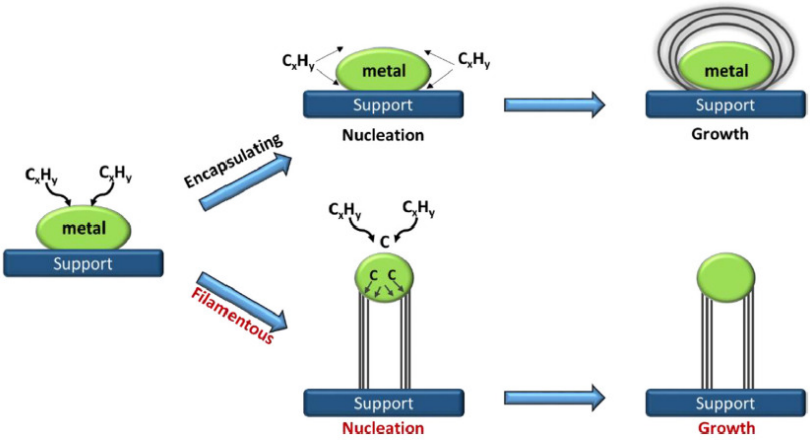

Figure 36: Schematic presentation of the growth mechanism of encapsulating and filamentous carbon due to carbon deposition in reforming systems [43].

10 Conclusion

The investigation of ethanol steam reforming using 20Co20Ni and 35Co05Ni catalysts has yielded significant findings. Firstly, the experimental results indicate a strong dependence on ethanol concentration for the 20Co20Ni catalyst, with an order of 1.06. This suggests that higher ethanol concentrations contribute to a faster ethanol steam reforming rate compared to the 35Co05Ni catalyst, which exhibited an order of 0.92. Controlling ethanol concentration is crucial for optimizing hydrogen production efficiency in this process.

Furthermore, the hydrogen reaction order provides valuable insights into catalyst performance. The 20Co20Ni catalyst displays a more negative hydrogen reaction order (-1.74) compared to the 35Co05Ni catalyst (-0.81). This indicates that the 20Co20Ni catalyst is more responsive to changes in hydrogen concentration, resulting in a faster rate of hydrogen production. The sensitivity of the 20Co20Ni catalyst to hydrogen concentration is a favorable characteristic for efficient hydrogen generation.

In addition to the dependence on ethanol and hydrogen concentration, the conversion rates of the catalysts were evaluated. The experimental data clearly demonstrate a higher conversion rate with the 20Co20Ni catalyst compared to the 35Co05Ni catalyst. This suggests that the specific composition of the 20Co20Ni catalyst is more favorable for the ethanol steam reforming reaction, leading to enhanced conversion efficiency. The higher conversion rate further supports the potential of the 20Co20Ni catalyst for hydrogen production.

Moreover, the activation energy of the catalysts was investigated to understand the energetics of the ethanol steam reforming process. The 20Co20Ni catalyst was found to have a lower activation energy compared to the 35Co05Ni catalyst. A lower activation energy indicates a more favorable reaction pathway, requiring less energy input to initiate and sustain the reaction. This finding suggests that the 20Co20Ni catalyst offers an energetically more efficient route for ethanol steam reforming, which is beneficial for industrial-scale hydrogen production processes.

In conclusion, the experimental investigation highlights the significance of ethanol concentration, hydrogen reaction order, conversion rates, and activation energy in ethanol steam reforming. The 20Co20Ni catalyst exhibits a strong dependence on ethanol concentration, higher sensitivity to changes in hydrogen concentration, higher conversion efficiency, and a more favorable reaction pathway with a

lower activation energy. These findings provide valuable insights for the development of efficient catalysts and processes in the field of renewable energy production, particularly in the context of ethanol steam reforming for hydrogen production.

References

[1] International Energy Agency. (2019, March) *Global Energy and CO2 Status Report 2019* , https://www.iea.org/reports/global-energy-co2-status-report-2019. Retrieved April 24, 2023, from https://www.iea.org/reports/global-energy-co2-status-report-2019.

[2] United Nations. (2019) *World Population Prospects 2019:Highlights (ST/ESA/SER.A/423)*

[3] Intergovernmental Panel on Climate Change (IPCC). (2018). Global Warming of 1.5°C., https://www.ipcc.ch/sr15/

[4] US Department of Energy. (2021). Hydrogen Fuel Basics, https://www.energy.gov/eere/fuelcells/hydrogen-fuel-basics

[5] United States Department of Energy (DOE). (2019) *Hydrogen Production: Natural Gas Reforming.*, https://www.energy.gov/eere/fuelcells/hydrogen-production-natural-gas-reforming

[6] Department of Agricultural and Biological Engineering, Mississippi State University, Mississippi 39762 *[Agus Haryanto, Sandun Fernando, Naveen Murali, and Sushil Adhikari]. (2005, March 3).*, Current Status of Hydrogen Production Techniques by Steam Reforming of Ethanol.

[7] Department of Mechanical Engineering, The University of Hong Kong, Pokfulam Road, Hong Kong, PR China*[Meng Ni, Dennis Y.C. Leung, Michael K.H. Leung]. (2006, August 7).* , A review on reforming bio-ethanol for hydrogen production.

[8] Applied Catalysis B: Environmental 2003, *Liguras DK, Kondarides DI, Verykios XE* , Production of hydrogen for fuel cells by steam reforming of ethanol over supported noble metal catalysts.

[9] Catal Commun 2004 , *Frusteri F, Freni S, Spadaro L, Chiodo V, Bonura G, Donato S. et al* , Hydrogen production for MC fuel cell by steam reforming of ethanol over MgO supported Pd, Rh, Ni and Co catalysts.

[10] Catal Today 2006*Erdohelyi A, Rasko J, Kecskes T, Toth M, Domok M, Baan K.*, Hydrogen formation in ethanol reforming on supported noble metal catalysts.

[11] J Catal 2005 *Aupretre F, Descorme C, Duprez D, Casanave D, Uzio D*, Ethanol steam reforming

[12] J Catal 2006 *Kugai J, Subramani V, Song C, Engelhard MH, Chin YH.B*, Effects of nanocrystalline CeO2 supports on the properties and performance of Ni–Rh bimetallic catalyst for oxidative steam reforming of ethanol

[13] J Mol Catal A Chem 2006 *Casanovas A, Llorca J, Homs N, Fierro JL, de la Piscina PR* , Ethanol reforming processes over ZnO-supported palladium catalysts: effect of alloy formation.

[14] Int J Hydrogen Energy 2005*Sun J, Qiu XP, Wu F, Zhu WT*, H2 from steam reforming of ethanol at low temperature over Ni/Y2O3, Ni/La2O3 and Ni/Al2O3 catalysts for fuel-cell application.

[15] Chem Eng J 2004 (1 *Comas J, Marino F, Laborde M, Amadeo N*, Bio-ethanol steam reforming on Ni/Al2O3 catalyst.

[16] Int J Hydrogen Energy 2006 *Yang Y, Ma JX, Wu F.* , Production of hydrogen by steam reforming of ethanol over a Ni/ZnO catalyst.

[17] Appl Catal A Gen 2004 *Frusteri F, Freni S, Chiodo V, Spadaro L, Blasi OD, Bonura G, Cavallaro S.* , Steam reforming of bio-ethanol on alkali-doped Ni/MgO catalysts: hydrogen production for MC fuel cell

[18] Int J Hydrogen Energy 2006 *Frusteri F, Freni S, Chiodo V, Donato S, Bonura S, Cavallaro S.*, Steam and auto-thermal reforming of bio-ethanol over MgO and CeO2 Ni supported catalysts

[19] Appl Cat A Gen 2005 *Akande AJ, Idem RO, Dalai AK.*, Synthesis, characterization and performance evaluation Ni/Al2O3 catalysts for reforming of crude ethanol for hydrogen production.

[20] Appl Catal A Gen 2006 *Barroso MN, Gomez MF, Arrua LA, Abello MC*, Hydrogen production by ethanol reforming over NiZnAl catalysts.

[21] Universität Osnabrück, 2007 *A. Greuling*, Röntgenstrukturanalyse von Isolatorschichten, Master's thesis

[22] Li He, De Chen, Esther Ochoa-Fernandez, Edd A. Blekkan,. (2009, January 21) *Co–Ni Catalysts Derived from Hydrotalcite-Like Materials for Hydrogen Production by Ethanol Steam Reforming*

[23] Cavani F, Trifiro F, Vaccari A (1991) Catal Today

[24] PDF-2 (1994) Joint Committee on Powder Diffraction Standards, International Center of Diffraction Data, Park Lane Swarthmore, Pennsylvania, USA

[25] Yu JJ, Jiang Z, Zhu L, Hao ZP, Xu ZP (2006) J. Phys. Chem. B 110:4291

[26] Kawabata T, Shinozuka Y, Ohishi Y, Shishido T, Takaki K, Takehira K (2005) J Mol Catal A Chem 236:206

[27] Ochoa-Fernandez E, Lacalle-Vila C, Christensen KO, Walmsley JC, Ronning M, Holmen A, Chen D (2007) Top Catal 45:3

[28] Bellotto M, Rebours B, Clause O, Lynch J, Bazin D, Elkaim E (1996) J Phys Chem 100:8535

[29] Bartholomew CH (1990) Catal Lett 7:27

[30] Chmielarz L, Kustrowski P, Rafalska-Lasocha A, Dziembaj R (2003) Thermochim Acta 395:225

[31] Unnikrishnan R, Narayanan S (1999) J Mol Catal A Chem 144:173

[32] Melo F, Morlane´s N (2008) Catal Today 133–135:374

[33] Dipartimento di Chimica Industriale e dei Materiali Wale de1 Risorgimento 4,40136 BOLOGNA (Italy).*[F. Cavani, F. Trifirb, A. Vaccari]. (n.d.)*, HYDROTALCITE-TYPE ANlONlC CLAYS: PREPARATION, PROPERTIES AND APPLICATIONS.

[34] K.P. De Jong , J.W. Geus , Carbon nanofibers: catalytic synthesis and applications, Catal. Rev. 42 (2007) 481–510 .

[35] C. A. Stowell and B. A. Korgel, Nano Lett., 2005, 5, 1203.

[36] C.H. Bartholomew and R.J. Farrauto, Fundamentals of Industrial Catalytic Processes, 2nd ed.; Wiley: Hoboken, NJ, 2006.

[37] Chemical Kinetics: Arrhenius Equation. (n.d.). https://www.coursehero.com/sg/general-chemistry/arrhenius-equation/.

[38] Interface Science and Technology *[Soleiman Mosleh, Mehrorang Ghaedi]. (n.d.).*, Photocatalysis: Fundamental Processes and Applications.

[39] Department of Chemistry, National Taiwan Normal UniVersity, Taipei, Taiwan, and Institute of Molecular Science and Department of Applied Chemistry, National Chiao Tung UniVersity, Hsinchu, Taiwan [Jeng-Han Wang, C. S. Lee, and M. C. Lin]. (2008, November 24). Mechanism of Ethanol Reforming: Theoretical Foundations.

[40] Laboratorio de Procesos Catal ıticos, Departamento de Ingenier ıa Qu ımica, Facultad de Ingenier ıa, Universidad de Buenos Aires, Ciudad Universitaria, Pabell on de Industrias (1428), Buenos Aires, Argentina [Mas Veronica, Baronetti Graciela, Amadeo Norma , Laborde Miguel]. (2007, July 6). Ethanol steam reforming using Ni(II)-Al(III) layered double hydroxide as catalyst precursor Kinetic study.

[41] J. Sehested , Four challenges for nickel steam-reforming catalysts, Catal. Today 111 (2006) 103–110 .

[42] G. Wang , H. Wang , W. Li , Z. Ren , J. Bai , J. Bai , Efficient production of hydrogen and mul- ti-walled carbon nanotubes from ethanol over Fe/Al 2 O 3 catalysts, Fuel Process. Technol. 92 (2011) 531–540 .

[43] W.T. Reichle, Chemtech, 16 (1986) 58.